eLife

Reviewed Preprint
v1 • September 25, 2024
Not revised

Reviewed Preprint
v2 • December 9, 2025
Revised by authors

# Dual-modal metabolic analysis reveals hypothermia-reversible uncoupling of oxidative phosphorylation in neonatal brain hypoxia-ischemia

**Naidi Sun[1,2,*,†], Yu-Yo Sun[3,4,5,†], Rui Cao[2], Hong-Ru Chen[4,5,6], Yiming Wang[2], Elizabeth Fugate[7], Marchelle R Smucker[4,5], Yi-Min Kuo[8], P Ellen Grant[9], Diana M Lindquist[7], Chia-Yi Kuan[4,5] ✉, Song Hu[1] ✉**

[1]Department of Biomedical Engineering, Washington University in St. Louis, St Louis, United States • [2]Department of Biomedical Engineering, University of Virginia, Charlottesville, United States • [3]Institute of BioPharmaceutical Sciences, National Sun Yat-Sen University, Kaohsiung, Taiwan • [4]Department of Neuroscience, University of Virginia, Charlottesville, United States • [5]Center for Brain Immunology and Glia (BIG), University of Virginia, Charlottesville, United States • [6]Department of Life Sciences and Institute of Genome Sciences, National Yang Ming Chiao Tung University, Taipei City, Taiwan • [7]Department of Radiology, Cincinnati Children's Hospital Medical Center, Cincinnati, United States • [8]Department of Anesthesiology, Taipei Veterans General Hospital; Department of Anesthesiology, College of Medicine, National Yang Ming Chiao Tung University, Taipei City, Taiwan • [9]Fetal-Neonatal Neuroimaging & Developmental Science Center, Boston Children's Hospital, Boston, United States

**For correspondence:**
alex.kuan@virginia.edu
songhu@wustl.edu

* Present address: Key Laboratory of Brain Health Intelligent Assessment and Intervention of the Ministry of Education, School of Medical Technology, Beijing Institute of Technology, Beijing, China

† These authors contributed equally to this work.

**Competing interests:** No competing interests declared

**Funding:** See page 22

**Reviewing editor:** Yamini Dalal, National Cancer Institute, United States



## eLife Assessment

This is an **important** study that utilized in vivo optical measurements of the cortical metabolic rate of O2 and blood flow, as well as measurements in isolated mitochondria to assess the uncoupling of the oxidative phosphorylation due to hypoxia-ischemia injury of the neonatal brain, and effects of the hypothermia treatment. The combination of state-of-the-art optical measurements, mitochondrial assays, and the use of various control experiments provides **convincing** evidence for the derived conclusions. This work will be of interest to those in the mitochrondrial metabolomics, brain injury and hypoxia fields.

https://doi.org/10.7554/eLife.100129.2.sa3

## Abstract

Hypoxia-ischemia (HI), which disrupts the oxygen supply-demand balance in the brain by impairing blood oxygen supply and the cerebral metabolic rate of oxygen ($CMRO_2$), is a leading cause of neonatal brain injury. However, it is unclear how post-HI hypothermia helps to restore the balance, as cooling reduces $CMRO_2$. Also, how transient HI leads to secondary energy failure (SEF) in neonatal brains remains elusive. Using photoacoustic microscopy, we examined the effects of HI on $CMRO_2$ in awake 10-day-old mice, supplemented by bioenergetic analysis of purified cortical mitochondria. Our results show that while HI suppresses ipsilateral $CMRO_2$, it sparks a prolonged $CMRO_2$-surge post-HI, associated with increased mitochondrial oxygen consumption, superoxide emission, and reduced mitochondrial membrane potential necessary for ATP synthesis—indicating oxidative phosphorylation (OXPHOS) uncoupling. Post-HI hypothermia prevents the $CMRO_2$-surge by constraining oxygen extraction fraction, reduces mitochondrial oxidative stress, and maintains ATP and N-acetylaspartate levels, resulting in attenuated infarction at 24 hours post-HI. Our findings suggest that OXPHOS-uncoupling induced by the post-HI $CMRO_2$-surge underlies SEF and blocking the surge is a key mechanism of hypothermia protection. Also, our study highlights the potential of optical $CMRO_2$-measurements for detecting neonatal HI brain injury and guiding the titration of therapeutic hypothermia at the bedside.

## Introduction

The human brain constitutes only 2% of the body mass, but utilizes ~20% of body's oxygen consumption (Rolfe and Brown, 1997). Disruptions in cerebral blood flow and oxygen supply cause a spectrum of brain injuries, including adult ischemic stroke and neonatal hypoxic-ischemic encephalopathy (HIE) (Allen and Brandon, 2011). In adult ischemic stroke, a >60% reduction in the cerebral metabolic rate of oxygen ($CMRO_2$) is indicative of looming infarction (Lee et al., 2003; Lin and Powers, 2018). However, the impacts of HIE on cerebral oxygen metabolism are far less certain due to the challenge of measuring $CMRO_2$ in infant brains by magnetic resonance imaging (MRI) or positron emission tomography (PET). Studies in animal models of HIE have revealed an initial recovery of brain adenosine triphosphate (ATP) levels during a short latent period after hypoxia-ischemia (HI), followed by a precipitous decline known as the secondary energy failure (SEF) that signifies looming infarction (Blumberg et al., 1997; Yager et al., 1992). However, the mechanisms of post-HI SEF and how therapeutic hypothermia protects neonatal brains against HI injury remain uncertain (Gunn et al., 2017). Also, it is unclear whether $CMRO_2$-measurments with recently developed bedside optical instruments, free of MRI's susceptibility to infant motion and PET's radiotoxicity, can detect HIE brain injury in a manner similar to adult ischemic stroke (De Carli et al., 2019; Dehaes et al., 2014; Ferradal et al., 2017; Jain et al., 2014).

Mitochondrial bioenergetics is vital to cellular functions and survival, and dysregulated oxidative-phosphorylation (OXPHOS) may promote neonatal HI brain injury (Niatsetskaya et al., 2012). While the phosphorylation efficiency of mitochondrial respiration (P/O ratio) remains stable over a wide range of substrate concentrations, it declines under hypoxia through a process known as OXPHOS-uncoupling (Kramer and Pearlstein, 1983), which is indicated by the rise of oxygen consumption despite a reduction of the mitochondrial membrane potential that is needed for ATP synthesis (Kristián and Siesjö, 1998). Although OXPHOS-uncoupling has been implicated in decoupling the contractive strength from oxidative metabolism after cardiac ischemia (Benzi and Lerch, 1992; Juhaszova et al., 2004), its role in HIE is unknown. We hypothesized that OXPHOS-uncoupling may be associated with mitochondrial injury in HIE, serving as the cause of post-HI SEF and a target for therapeutic hypothermia.

To test this hypothesis, we applied a head-restrained photoacoustic microscopy (PAM) technique to measure $CMRO_2$ during and immediately after HI in awake 10-day-old (P10) mice. Using multi-parametric PAM, we simultaneously acquired high-resolution images of cerebral blood flow (CBF), the oxygen saturation of hemoglobin ($sO_2$), and the total concentration of hemoglobin ($C_{Hb}$), which can be combined to calculate $CMRO_2$ in absolute values (Figure 1A and see Methods for details of the PAM system). The use of awake mouse neonates avoided the confounding effects of anesthesia on CBF and $CMRO_2$ (Cao et al., 2017; Gao et al., 2017; Sciortino et al., 2021; Slupe and Kirsch, 2018). In addition, we measured the oxygen consumption rate (OCR), reactive oxygen species (ROS), and the membrane potential of mitochondria that were immediately purified from the same cortical area imaged by PAM. This dual-modal analysis enabled a direct comparison of cerebral oxygen metabolism and cortical mitochondrial respiration in the same animal. Moreover, we compared the effects of therapeutic hypothermia on oxygen metabolism and mitochondrial respiration and correlated the extent of $CMRO_2$-reduction with the severity of infarction at 24 hours after HI. Our results suggest that blocking HI-induced OXPHOS-uncoupling is an acute effect of hypothermia and that optical detection of $CMRO_2$ may have clinical applications in HIE.

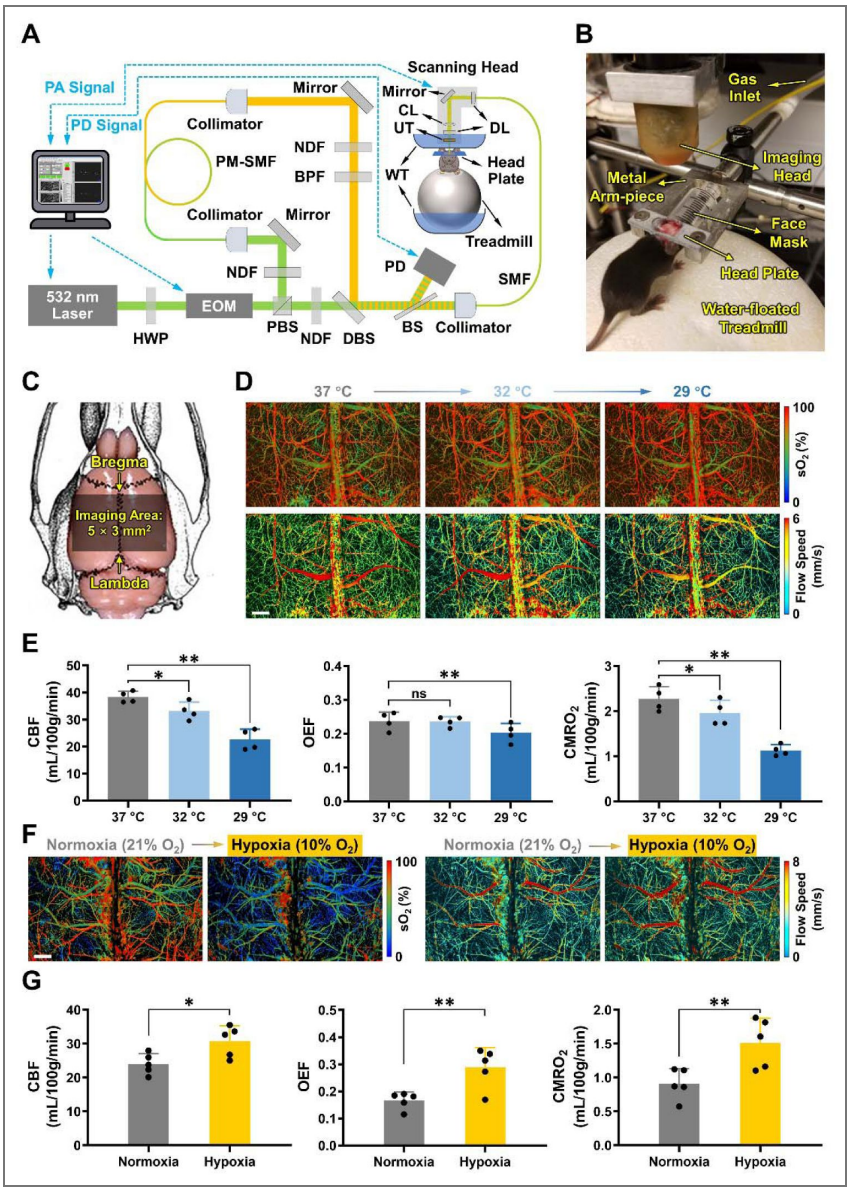


**Figure 1. Multi-parametric photoacoustic microscopy (PAM) of hemodynamic and oxygen-metabolic responses of uninjured neonatal mouse brains to hypothermia or hypoxia.**

(**A**) Schematic of the head-restrained multi-parametric PAM system. PA, photoacoustic; PD, photodiode; HWP, half-wave plate; EOM, electro-optical modulator; PBS, polarizing beam splitter; NDF, neutral-density filter; PM-SMF, polarization-maintaining single-mode fiber; BPF, band-pass filter; DBS, dichroic beam splitter; BS, beam sampler; SMF, single-mode fiber; DL, doublet; CL, correction lens; UT, ring-shaped ultrasonic transducer; WT, water tank. (**B**) Photograph of the placement of an awake 10-day-old (P10) mouse wearing the head plate in the PAM system. Note that the water tank is removed to better show the mouse and related parts for head-restrained awake-brain imaging. (**C**) Illustration of the imaging field (5 × 3 $mm^2$) that covers both hemicortices between the Bregma and Lambda on the skull of mouse neonates. (**D**) Multi-parametric PAM images of the oxygen saturation of hemoglobin ($sO_2$) and blood flow speed in an awake P10 mouse, with the skull temperature set at 37, 32, and 29 °C, respectively. Scale bar: 500 μm. (**E**) Hemodynamic and oxygen-metabolic responses of the neonatal mouse cortex to different skull temperatures, including cerebral blood flow (CBF), oxygen extraction fraction (OEF), and the cerebral metabolic rate of oxygen ($CMRO_2$). Gray bars: 37 °C; light blue bars: 32 °C; dark blue bars: 29 °C. One-way ANOVA was performed, and data are presented as mean ± standard deviation (n = 4). ns, no significance; *, $p < 0.05$; **, $p < 0.01$. (**F**) Multi-parametric PAM images of $sO_2$ and blood flow speed in an anesthetized P10 mouse under normoxia (inhaled oxygen concentration: 21%) versus hypoxia (inhaled oxygen concentration: 10%). Scale bar: 500 μm. (**G**) Hemodynamic and oxygen-metabolic responses of the neonatal mouse cortex to normoxia *vs.* hypoxia, including CBF, OEF, and $CMRO_2$. Gray bars: normoxia; orange bars: hypoxia. Student t-test was performed, and data are presented as mean ± standard deviation (n = 5). *, $p < 0.05$; **, $p < 0.01$.

# Results

## Effects of Cooling and Hypoxia on $CMRO_2$ in Uninjured Mouse Neonates

First, we studied the effects of hypothermia alone on neonatal $CMRO_2$. As shown in Figure 1A and B, an awake P10 mouse was placed between the PAM apparatus and a water-floated voluntary treadmill, with the temperature of the water tank above the mouse head adjusted to achieve normothermia or hypothermia based on the skull temperature (Figure S1). Note that while the mouse skull was exposed, no craniotomy was necessary. Multi-parametric PAM images over a 5 × 3 $mm^2$ region from the Bregma to Lambda in both cortices were acquired within 40 minutes (Figure 1C). Using this system, we assessed the effects of hypothermia (from 37 °C to 32 °C to 29 °C of the mouse skull temperature) on $CMRO_2$ in uninjured mice (Figure 1D). Quantitative analysis revealed a decline in CBF from 38.37 mL/100g/min at 37 °C to 33.18 mL/100g/min at 32 °C (86% of the baseline) and to 22.65 mL/100g/min at 29 °C (59% of the baseline) (Figure 1E, left). In contrast, OEF remained unchanged at 32 °C and slightly declined to 85% of the baseline at 29 °C (Figure 1E, middle). Consequently, $CMRO_2$ declined from 2.27 mL/100g/min at 37 °C to 1.97 mL/100g/min at 32 °C (86% of the baseline) and further to 1.13 mL/100g/min at 29 °C (50% of the baseline) (Figure 1E, right). These results show that hypothermia reduces $CMRO_2$ in uninjured mouse neonates, primarily through the suppression of CBF.

Next, we studied the effects of hypoxia alone on neonatal $CMRO_2$. Exposing anesthetized P10 mice to hypoxia (10% $O_2$) resulted in an increase of $CMRO_2$ (from 0.91 to 1.51 mL/100g/min), which was attributed to the rise in both CBF (from 24.04 to 30.74 mL/100g/min) and OEF (from 0.17 to 0.29) (Figure 1F and G). While this observation of greater oxygen consumption under a lower oxygen tension is seemingly counterintuitive, it aligns with the previous reports of higher $CMRO_2$ and cytochrome c oxidase activity in mild hypoxia (Tsuji et al., 1995; Vestergaard et al., 2016). This phenomenon is presumably due to an increased cerebral energy demand under hypoxia.

## Effects of Combined HI on $CMRO_2$ and Mitochondrial Respiration

Then, we studied the effects of combined HI under the Vannucci model, which involves unilateral common carotid artery (CCA) occlusion and transient hypoxia (Kuan et al., 2021; Yang et al., 2009). Using time-lapse PAM, we compared the dynamic changes of CBF, OEF, and $CMRO_2$ in the two hemicortices from unilateral CCA-ligation to combined HI (40 minutes), and for 2 hours upon returning to normoxia in awake P10 mice (Figure 2A–D and Table S1).

Before the onset of hypoxia, CCA-ligation alone did not provoke a significant difference in $CMRO_2$ between the two hemicortices (1.56 *vs.* 1.26 mL/100g/min; *p*-value, 0.6107; the first pair of red and green points in Figure 2D). When hypoxia was initiated, however, the contralateral (CL) cortex had a significant increase in $CMRO_2$, similar to the responses in uninjured mice, while the CCA-ligated counterpart showed a marked reduction in $CMRO_2$ (0.78 *vs.* 2.37 mL/100g/min; *p*-value, 0.0011; the second pair of red and green points in Figure 2D). Upon switching back to normoxia, $CMRO_2$ in the CL cortex quickly returned to the pre-hypoxia level and rose slowly afterwards, while $CMRO_2$ in the ipsilateral (IL) cortex rapidly rebounded above the pre-hypoxia level and remained elevated for at least 2 hours (the last three red and green points in Figure 2D).

To determine the causes of the post-HI $CMRO_2$-surge, we recorded electroencephalography (EEG) of the P10 mouse before, during, and after HI to test whether the surge was due to status epilepticus (Lin and Powers, 2018). Although showing seizure-like behaviors and a few spike-wave discharges on top of the EEG-suppression during HI (Figure 2E, hypoxia), mice only showed a gradual recovery from the suppression without burst discharges on EEG post-HI (Figure 2E, normoxia). Thus, the post-HI $CMRO_2$-surge was not attributed to status epilepticus.

We then isolated the mitochondria from both hemicortices of injured mouse brains at 2 or 5 hours post-HI and from the uninjured (UN) mouse brains for *in-vitro* analysis (see Materials and Methods for details of the mitochondrial function analysis). At 2 hours post-HI, mitochondria from the IL

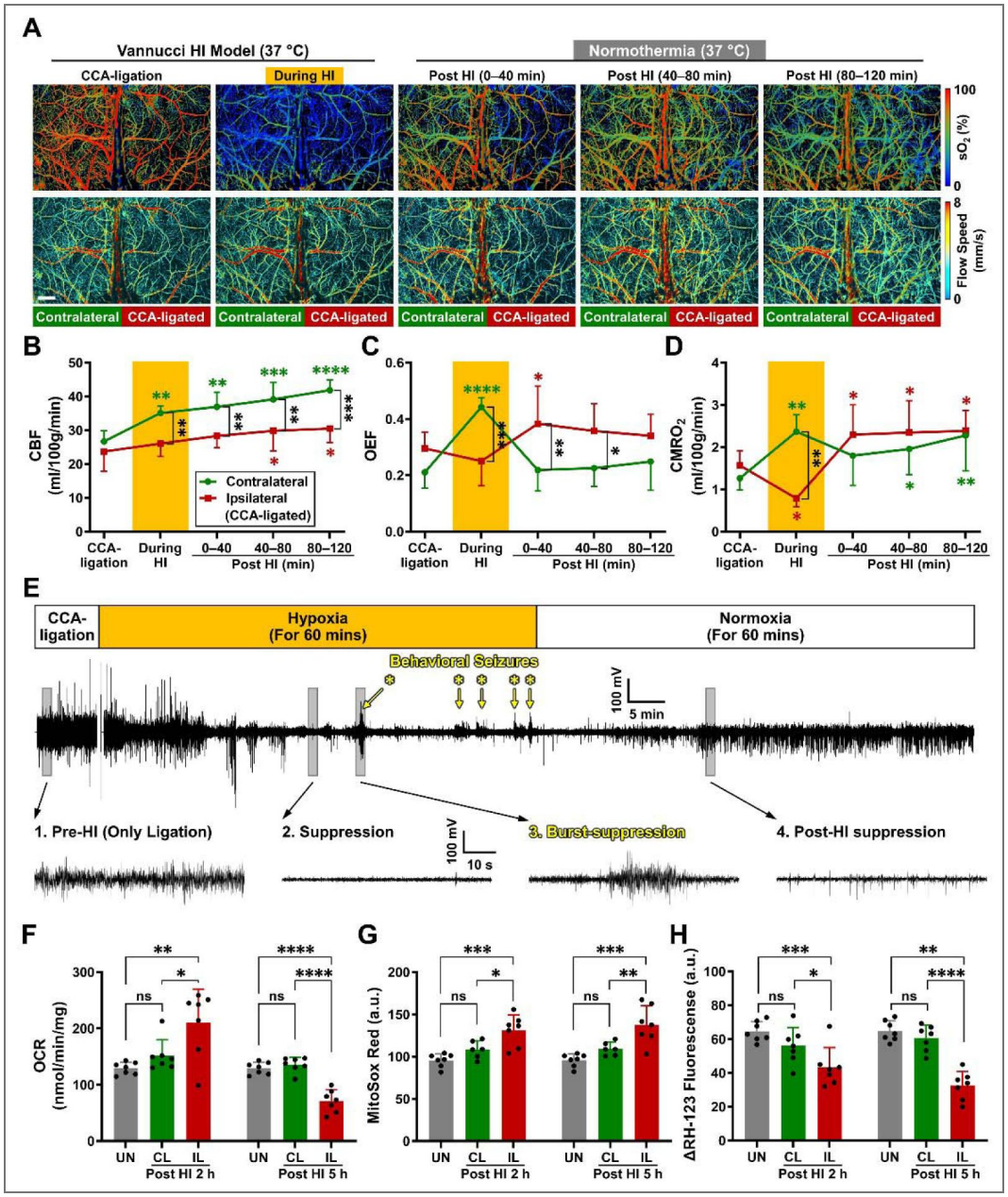


**Figure 2. Effects of combined hypoxia-ischemia (HI) on cerebral hemodynamics, oxygen metabolism, and mitochondrial bioenergetics in mouse neonates under normothermia.**

(**A**) Time-lapse PAM images of the oxygen saturation of hemoglobin ($sO_2$) and blood flow speed in an awake P10 mouse during unilateral CCA-ligation, combined HI, as well as 0–40, 40–80, and 80–120 minutes post-HI. Scale bar: 500 μm. (**B–D**) Hemodynamic and oxygen-metabolic responses of the contralateral (green line and symbols) and ipsilateral (red line and symbols) cortices to the Vannucci HI Model under normothermia, including (**B**) cerebral blood flow (CBF), (**C**) oxygen extraction fraction (OEF), and (**D**) the cerebral metabolic rate of oxygen ($CMRO_2$). Green and red asterisks indicate the statistical significance, if any, over the baseline (i.e., CCA-ligation alone) values measured in the same animal, while black asterisks indicate the statistical significance, if any, between the measurements in the two hemicortices at the same time point. Two-way ANOVA was performed, and data are presented as mean ± standard deviation (n = 5). *, $p < 0.05$; **, $p < 0.01$; ***, $p < 0.001$; ****, $p < 0.0001$. (**E**) Electroencephalography (EEG) recording of the ipsilateral cortex in a P10 mouse right after the unilateral CCA-ligation, 60-minute hypoxia (inhaled oxygen concentration: 10%), and 60-minute normoxia (inhaled oxygen concentration: 21%). Zoom-in views of the boxed regions show characteristic EEG patterns, including 1. pre-HI baseline, 2. Suppression, 3. burst-suppression correlated with seizure behaviors (highlighted by yellow asterisks), and 4. post-HI suppression. n = 6. (**F–H**) Comparison of the mitochondrial parameters acquired in the uninjured (UN, gray bars), contralateral (CL, green bars), and ipsilateral (IL, red bars) cortices at 2 or 5 hours post-HI, including (**F**) oxygen consumption rate (OCR), (**G**) MitoSox Red, and (**H**) ΔRH-123 fluorescence. One-way ANOVA was performed, and data are presented as mean ± standard deviation (n = 7). ns, no significance; *, $p < 0.05$; **, $p < 0.01$; ***, $p < 0.001$; ****, $p < 0.0001$.

cortex showed increased OCR (Figure 2F and Figure S2) and superoxide (as measured by the MitoSox Red fluorescence, Figure 2G), but reduced mitochondrial membrane potential ($\psi_m$, as measured by the ΔRH-123 fluorescence, Figure 2H), compared to mitochondria in the CL cortex or the UN brain. By 5 hours post-HI, mitochondria in the IL cortex manifested a lower OCR and $\psi_m$, but an even higher superoxide emission, suggesting more substantial mitochondria injury (Figure 2F–H). In contrast, mitochondria in the CL cortex at both 2 and 5 hours post-HI showed comparable OCR, superoxide, and $\psi_m$ to those from the UN brain (Figure 2F–H). These results suggest that post-HI $CMRO_2$-surge can be attributed to OXPHOS-uncoupling and ROS-emission, which may promote mitochondrial injury.

## Effects of Hypothermia Treatment on HI-induced $CMRO_2$ Surge and Mitochondria Injury

Next, we tested the effects of therapeutic hypothermia on $CMRO_2$ and mitochondrial functions. To mimic clinical settings, CCA-ligation and combined HI were performed at the room temperature, while hypothermia was initiated after HI by reducing the mouse skull temperature from 37 °C to 32 °C (Figure 3A–D).

Similar to Figure 2D, HI provoked a rise of $CMRO_2$ in the CL cortex and a decline of $CMRO_2$ in the IL cortex (Figure 3D). Notably, post-HI hypothermia blunted the $CMRO_2$-surge in the IL cortex, locking it at the pre-HI level throughout the 2-hour monitoring period (Figure 3D and Table S2). Comparison of the PAM measurements obtained under normothermia *vs.* hypothermia revealed that the chief effect of hypothermia was to block the rise of post-HI OEF rather than reducing CBF (Figure 3E), as observed in the uninjured neonates (Figure 1E). Similar to our results, a recent study also showed minimal reduction of post-HI CBF by hypothermia at 32 °C (Buckley et al., 2015).

We then tested whether therapeutic hypothermia protects mitochondria and prevents the onset of SEF, as previously postulated (Gunn et al., 2017). We isolated mitochondria from the CL and IL cortex, with or without the 4-hour hypothermia treatment for *in-vitro* analysis at 5 hours post-HI (i.e., 1 hour after the conclusion of the hypothermia treatment). As shown in Figure 3F–I, mitochondria isolated from the IL cortex without hypothermia treatment showed reduced OCR, higher superoxide, as well as lower hydrogen peroxide ($H_2O_2$) and mitochondria $\psi_m$, compared to those receiving hypothermia treatment or from the CL cortex. In contrast, mild hypothermia (32 °C) had no suppressive effects on OCR, superoxide and $H_2O_2$ emission, and $\psi_m$ of mitochondria in the CL cortex. We also compared the mitochondrial ATP levels at 6 hours post-HI and found a higher ATP level (0.64 μmol/g) in the IL cortex receiving hypothermia treatment than those without hypothermia (0.33 μmol/g, Figure 3J). These results confirmed that therapeutic hypothermia maintained mitochondrial OCR and $\psi_m$, reduced superoxide and $H_2O_2$ emission, and prevents post-HI SEF. In addition, *in vivo* proton MRS in infants with HIE has also shown a reduction in NAA, particularly in cases of severe injury (Lally et al., 2019). This reduction in NAA, observed in neonatal intensive care settings, reflects neuronal and axonal loss or dysfunction and serves as a biomarker for injury severity. The alignment between our *ex vivo* observations and *in vivo* MRS findings in clinical studies reinforces the translational relevance of our model for investigating metabolic disturbances in neonatal HIE.

## Using Optically Measured $CMRO_2$ to Detect Neonatal HI Brain Injury

Finally, we compared $CMRO_2$ and brain infarction with or without hypothermia treatment at 24 hours after HI. PAM measurements (Figure 4A) and tissue-level $CMRO_2$ mapping (Figure 4B) showed better preservation of oxygen metabolism in the IL cortex of hypothermia-treated mice, compared with those without the treatment. Notably, the marked reduction of $CMRO_2$ at 24 hours post-HI in non-treated mice (Figure 4B) was coupled to impaired triphenyl-tetrazolium chloride (TTC) staining, which corresponded to tissue infarction (Figure 4C). The TTC analysis confirmed the reduction of infarct size in mice receiving therapeutic hypothermia than those without (8.74

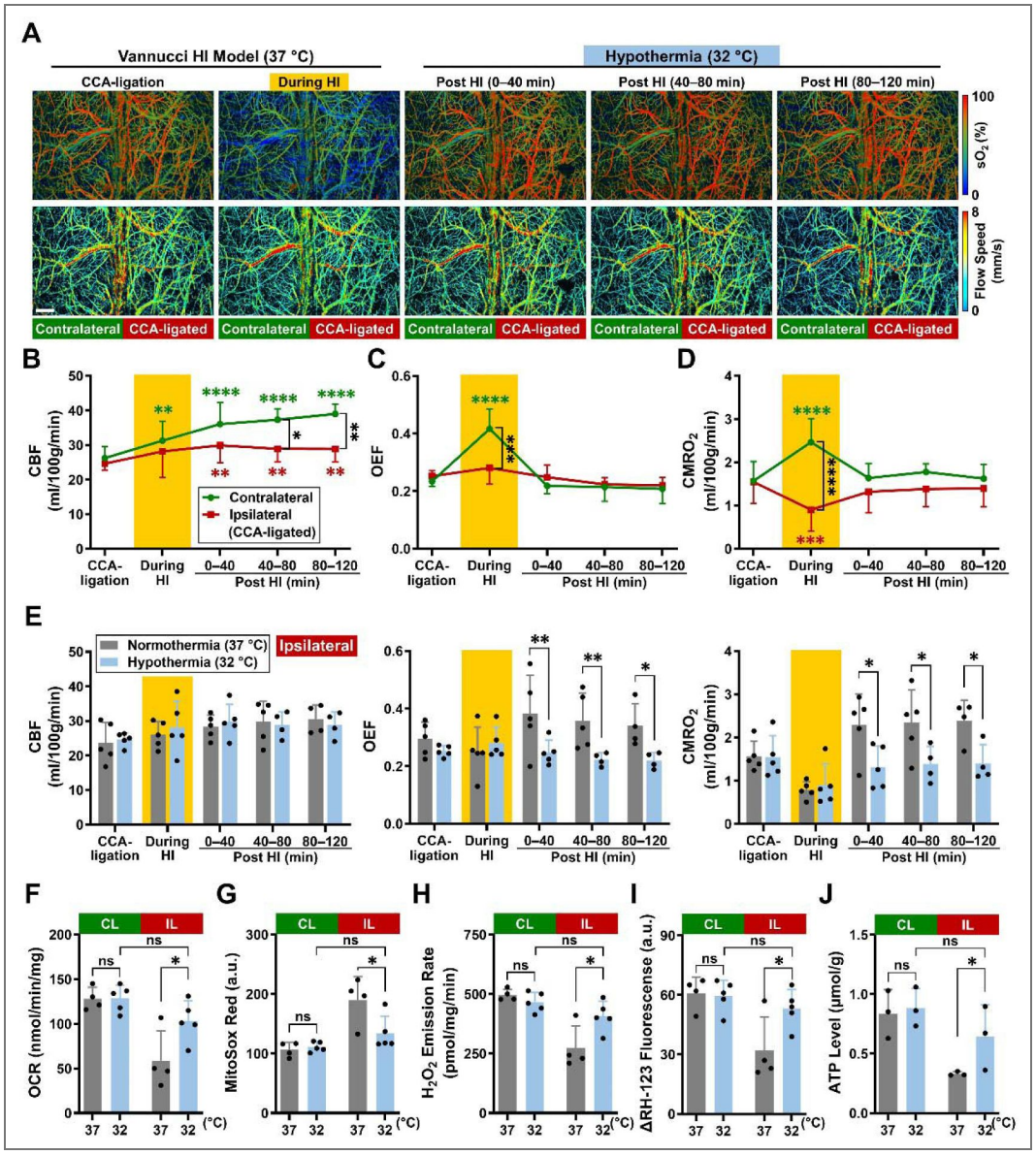


**Figure 3. Effects of hypoxia-ischemia (HI) on cerebral hemodynamics, oxygen metabolism, and mitochondrial bioenergetics in mouse neonates under hypothermia *vs.* normothermia.**

(**A**) Time-lapse PAM images of the oxygen saturation of hemoglobin ($sO_2$) and blood flow speed in an awake P10 mouse during unilateral CCA-ligation, combined HI, as well as 0–40, 40–80, and 80–120 minutes post-HI. Scale bar: 500 μm. (**B–D**) Hemodynamic and oxygen-metabolic responses of the contralateral (green line and symbols) and ipsilateral (red line and symbols) cortices to the Vannucci HI Model under hypothermia, including (**B**) cerebral blood flow (CBF), (**C**) oxygen extraction fraction (OEF), and (**D**) the cerebral metabolic rate of oxygen ($CMRO_2$). Green and red asterisks indicate the statistical significance, if any, over the baseline (i.e., CCA-ligation alone) values measured in the same animal, while black asterisks indicate the statistical significance, if any, between the measurements in the two hemicortices at the same time point. (**E**) Comparison of CBF, OEF, and $CMRO_2$ responses of the ipsilateral cortex to the HI insult under normothermia (37 °C, gray bars) *vs* hypothermia (32 °C, light blue bars). For (**B–E**), two-way ANOVA was performed, and data are presented as mean ± standard deviation (n = 5). *, $p < 0.05$; **, $p < 0.01$; ***, $p < 0.001$; ****, $p < 0.0001$. (*F–I*) Comparison of the mitochondrial parameters acquired in the contralateral (CL, green bars) and ipsilateral (IL, red bars) cortices at 5 hours post-HI under normothermia (37 °C, gray bars) *vs* hypothermia (32 °C, light blue bars), including (**F**) oxygen consumption rate (OCR), (**G**) MitoSox Red, (**H**) $H_2O_2$ emission rate, and (*I*) ΔRH-123 fluorescence. Two-way ANOVA was performed, and data are presented as mean ± standard deviation (n = 4 or 5 for normothermia or hypothermia treatment group, respectively). ns, no significance; *, $p < 0.05$. **(J)** Comparison of the ATP concentrations measured in the CL and IL cortices at 6 hours post-HI under normothermia (37 °C, gray bars) *vs* hypothermia (32 °C, light blue bars). Two-way ANOVA was performed, and data are presented as mean ± standard deviation (n = 3). ns, no significance; *, $p < 0.05$. For (**F–J**), the *in-vitro* analyses were performed in mitochondria isolated from HI-injured mice with or without a 4-hour hypothermia treatment, followed by another (**F–I**) one hour or (**J**) two hours recovery in normothermia.

$mm^3$*vs.* 45.25 $mm^3$, Figure 4D). Direct comparison of the hemodynamic and oxygen-metabolic parameters showed that post-HI hypothermia maintained CBF (41.13 mL/100g/min), OEF (0.23), and $CMRO_2$ (2.12 mL/100g/min) in the IL cortex to a level similar to those in the CL cortex (blue bars in Figure 4E–G). In contrast, mice without hypothermia treatment showed a marked reduction of OEF (0.04) and $CMRO_2$ (0.35 mL/100g/min) in the IL cortex at 24 hours post-HI (gray bars in Figure 4E–G).

Additionally, the proton nuclear magnetic resonance (NMR) analysis showed significant reductions of total creatine (Cr/PCr), choline (Cho), glutamate and glutamine (Glx), and NAA in the IL cortex, compared to those in the CL cortex, in mice without hypothermia treatment (Figure 4H and gray bars in Figure S3). In contrast, mice that received therapeutic hypothermia maintained similar levels of Cr/PCr, Cho, and NAA between the two hemicortices (Figure 4I and light blue bars in Figure S3). These results suggest that marked reduction of post-HI $CMRO_2$ signifies SEF and tissue infarction, similar to that in adult ischemic stroke (Lee et al., 2003; Lin and Powers, 2018).

# Discussion

Acute post-asphyxia HIE around the time of birth remains a major cause of neonatal death and lifelong neurological deficits. Clinical observations and animal studies suggest that brain cells initially recover from the insult during a short latent phase, typically lasting ~6 hours, but then enter a deterioration phase characterized by progressive failure of oxygen metabolism (i.e., SEF), seizures, and death (Blumberg et al., 1997; Gunn et al., 2017; Yager et al., 1992). Acute treatment with mild hypothermia (32–34 °C) prevents the onset of SEF in moderate HIE, but the mechanisms remain unclear for at least two reasons (Gunn et al., 2017). First, hypothermia normally inhibits instead of enhancing cerebral oxygen metabolism. Second, since mild hypothermia has little effect on the EEG activity (Erecinska et al., 2003), which does not support the common notion that it protects through suppression of neuronal activity and cerebral energy demand. In this study we combined PAM-based optical measurement of $CMRO_2$ and functional assays of acutely purified cortical mitochondria in HI-injured awake mouse neonates to investigate the causes of post-HI SEF and hypothermia protection. Our study has three unique features. First, awake-brain imaging avoids the confounding effects of anesthesia on CBF and $CMRO_2$ (Cao et al., 2017; Gao et al., 2017; Sciortino et al., 2021; Slupe and Kirsch, 2018). Second, our PAM-based $CMRO_2$-measurement is analogous to optical $CMRO_2$-detection using bedside instruments that may enable non-invasive monitoring of neonatal brain injury (De Carli et al., 2019; Dehaes et al., 2014; Ferradal et al., 2017; Jain et al., 2014; Liu et al., 2014a). Third, our experiments establish a direct connection between the impacts of HI on $CMRO_2$ and that on mitochondria, which account for the majority of cerebral oxygen metabolism (Rolfe and Brown, 1997). In the following, we discuss the implications of our findings on the cause of post-HI SEF, the protective mechanisms of hypothermia in HI, and the potential of optic $CMRO_2$-detection in neonatal care.

## Causes of post-HI SEF: uncoupled OXPHOS and excessive ROS

In normal conditions, $CMRO_2$ remains relatively stable over a range of CBF and brain glucose-uptake changes as the so-called “uncoupling of CBF and cerebral oxygen metabolism” (Fox and Raichle, 1986). The autoregulation of $CMRO_2$, accomplished by alterations of OEF (an index of oxygen diffusion across capillaries) in the opposite direction of CBF fluctuations, maintains a consistent level of mitochondrial respiration, while glycolysis and phosphocreatine-creatine conversion support the transient outbursts of neural activity (Chen et al., 2022; Lin and Powers, 2018).

As illustrated by our PAM measurements in unilateral CCA-ligation, the IL cortex showed OEF-elevation to compensate for a lower CBF than the CL cortex and maintained bilaterally similar $CMRO_2$ values (Figure 2D and 3D, and Table S1 and S2). During combined HI, the CL cortex showed up-regulation of both CBF and OEF and produced a higher $CMRO_2$, similar to the responses to moderate hypoxia (10% $O_2$) in uninjured animals (Figure 1G). These responses

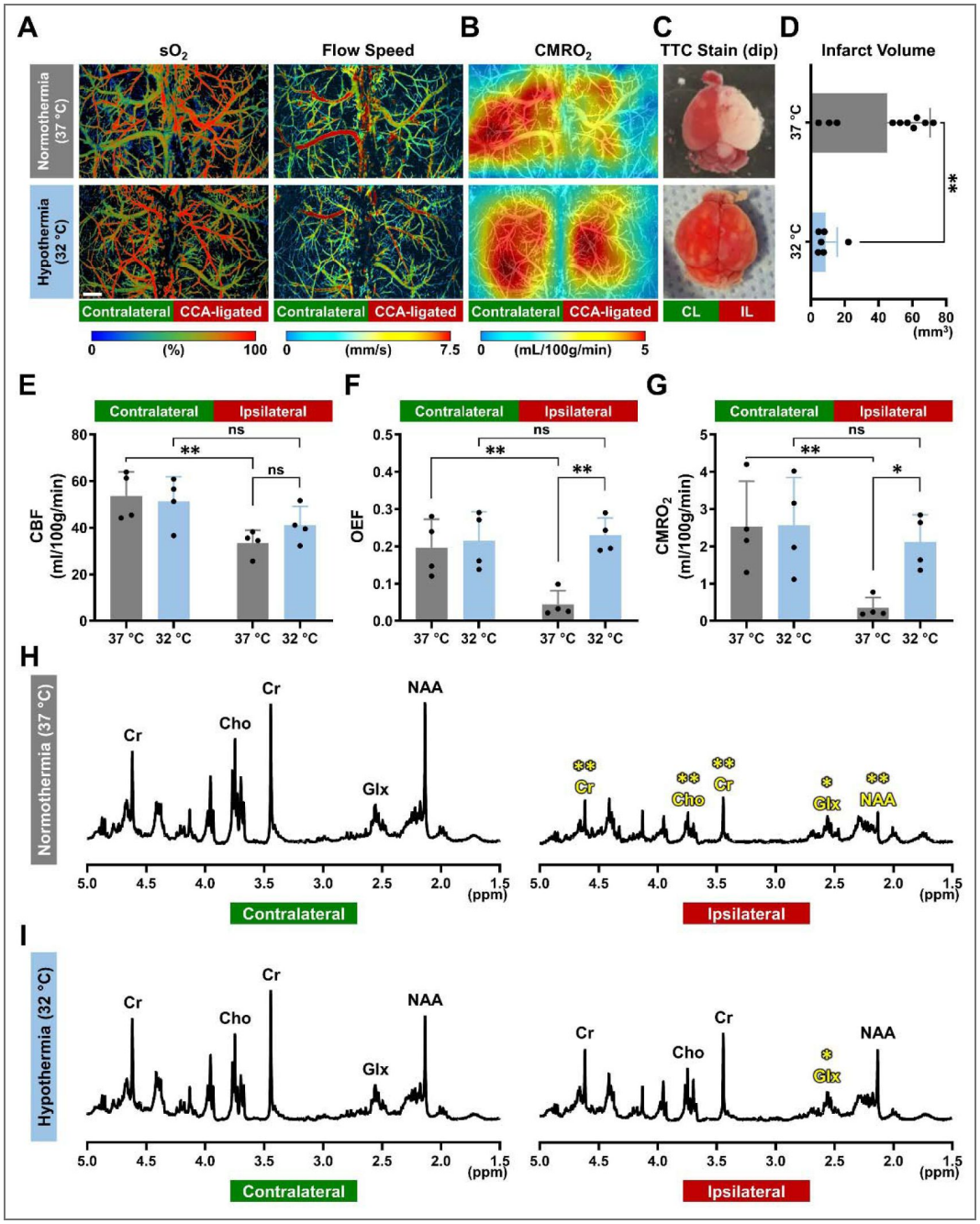


**Figure 4. Correlation of $CMRO_2$ and post-HI brain infarction in mouse neonates at 24 hours.**

(**A–C**) Multi-parametric PAM images of (**A**) the oxygen saturation of hemoglobin ($sO_2$) and blood flow speed and (**B**) the cerebral metabolic rate of oxygen ($CMRO_2$), as well as (**C**) the triphenyl-tetrazolium chloride (TTC) analysis of the dissected brain after completion of the *in vivo* PAM imaging at 24 hours post-HI. The top and bottom rows are data acquired in the neonate brain treated with normothermia (37 °C, upper row) or hypothermia (32 °C, lower row) for 4 hours, respectively. CL, contralateral; IL, ipsilateral. Scale bar: 500 μm. (**D**) Comparison of the infarct volume quantified based on the TTC analysis (n = 6 for the normothermia group and n = 10 for the hypothermia group). Student *t*-test was performed, and data are presented as mean ± standard deviation. **, $p < 0.01$. (**E–G**) Comparison of (**E**) cerebral blood flow (CBF), (**F**) oxygen extraction fraction (OEF), and (**G**) $CMRO_2$ acquired at 24 hours post-HI in the neonate brain treated with normothermia (37 °C, gray bars) or hypothermia (32 °C, light blue bars) for 4 hours. Two-way ANOVA was performed, and data are presented as mean ± standard deviation (n = 4). ns, no significance; *, $p < 0.05$; **, $p < 0.01$. (**H–I**) Characteristic proton-HRMAS spectra of the snap-frozen tissue from the contralateral and ipsilateral cortex extracted at 24 hours post-HI from HI-injured mice treated with (**H**) normothermia or (**I**) hypothermia. The spectra are scaled to the same peak height for myo-inositol. Cr, creatine and phosphocreatine; Cho, choline; Glx, glutamate and glutamine; NAA, N-acetyl aspartate. Two-way ANOVA was performed (n = 5 for normothermia and n = 3 for hypothermia). *, $p < 0.05$; **, $p < 0.01$.

suggest a greater demand of brain energy as adaptation to hypoxia. In contrast, the IL cortex showed a smaller increase of CBF and mild or no changes of OEF in combined HI, leading to a 40–50% reduction in $CMRO_2$ (Figure 2D and 3D, and Table S1 and S2). Consistent with our findings, previous studies showed marked reduction of ATP and phosphocreatine, as well as a massive buildup of lactate, in the IL cortex during combined HI, while the CL cortex showed only minimal ATP-reduction and modest accumulation of lactate (Chen et al., 2022; Gunn et al., 1997; Salford and Siesjö, 1974). The bilateral disparity of ATP homeostasis-versus-reduction during combined HI may influence the divergent $CMRO_2$ responses post-HI: the CL cortex showed $CMRO_2$ recovery to the pre-HI level because extra ATP-output is no longer required to cope with hypoxia, while the IL cortex developed a surge of mitochondrial respiration (and thus $CMRO_2$) presumably to recompense the energy deficit incurred during HI (Figure 2D and 2F).

Persistent increase in oxygen consumption, albeit to a lesser degree, was also observed in post-ischemic myocardium and after spreading depression in rodent cerebral cortex (Benzi and Lerch, 1992; Juhaszova et al., 2004; Piilgaard and Lauritzen, 2009). Moreover, brain-injured infants showed a higher $CMRO_2$ than healthy neonates (Grant et al., 2009), suggesting that the rebound of oxygen metabolism is a generic response to transient severe HI. Notably, our PAM measurements showed that the rise of post-HI $CMRO_2$ is primarily driven by the increase of OEF (Figure 2C and Table S1), which may be due to reduction of capillary transient time heterogeneity (Paulson et al., 2010). The HI-induced energy deficit and tissue hypoxia may also assist oxygen diffusion across capillaries to elevate the OEF (Chen et al., 2022; Salford and Siesjö, 1974; Yang et al., 2009). Finally, post-HI acidosis may also promote mitochondrial respiration (Jespersen and Østergaard, 2012; Khacho et al., 2014). We suggest that these cellular and vascular factors collectively promote mitochondrial respiration and $CMRO_2$ immediately after HI (Figure 5A).

However, the post-HI mitochondrial respiration has features of OXPHOS uncoupling and ROS release, as shown by the rise of oxygen consumption and mitochondrial superoxide despite the reduction of mitochondrial membrane potential needed for ATP-synthesis through F0/F1 ATPase (Figure 2F–H). The triggers of OXPHOS uncoupling after HI may include persistent tissue hypoxia (Kramer and Pearlstein, 1983; Kuan et al., 2021), influx of calcium in the mitochondrial matrix (Benzi and Lerch, 1992; Kristián and Siesjö, 1998), reverse electron transfer through Complex I (Kim et al., 2018), nitric oxide-mediated inhibition of the cytochrome oxidase in Complex IV (Cooper and Giulivi, 2007), and ROS-caused disruption of the electron transport chain super-complexes and mitochondrial cristae (Paradies et al., 2018), according to the literature and our results (Figure S4). Importantly, the release of extra ROS during uncoupled OXPHOS injures the mitochondria (Granger and Kvietys, 2015; Murphy, 2009), as indicated by the reduction of oxygen consumption and mitochondrial membrane potential at 5 hours post-HI, if without hypothermia treatment (Figure 2F–H). These results suggest that uncoupled OXPHOS and ROS-mediated injury of mitochondria are important mechanisms of post-HI SEF (Figure 5A).

## Protective mechanisms of hypothermia

If the aforementioned hypothesis is correct, therapeutic hypothermia shall attenuate the post-HI $CMRO_2$-surge. Indeed, our data showed that the initiation of mild hypothermia (32 °C) post-HI efficiently clamped the rebounding $CMRO_2$ to the pre-HI level at both hemicortices over the 2-hour PAM-monitoring period (Figure 3D). Furthermore, hypothermia blocked the rapid demise of mitochondria at 5 hours post-HI (Figure 3F–I) and preserved cortical ATPs at 6 hours post-HI (Figure 3J). In other words, neonatal mice recovering under mild hypothermia after HI escaped the initial overshoot of $CMRO_2$ and the subsequent SEF, as predicted by our hypothesis (Figure 5A).

In terms of mechanism, our PAM measurements showed that hypothermia mainly blocks the rise of post-HI OEF to constrain $CMRO_2$ (Figure 3E and Table S2). This is different from the responses to mild hypothermia (32 °C) in uninjured mice, which showed CBF-reduction but negligible changes in OEF (Figure 1E). This difference suggests unique effects of hypothermia in

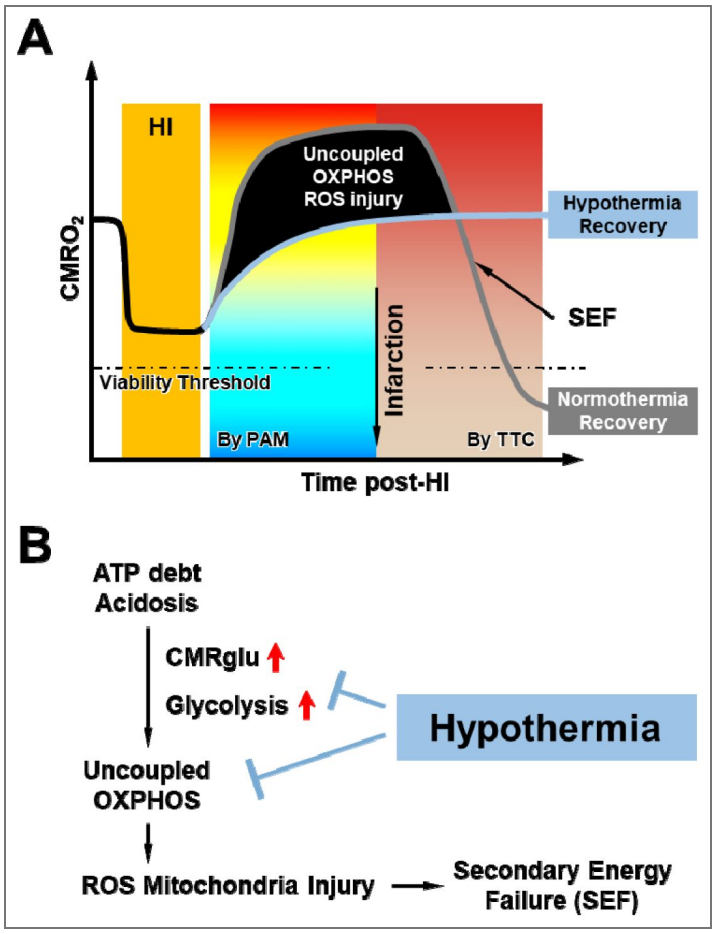


**Figure 5. Schematic conclusion and open questions.**

(**A**) Combined hypoxia-ischemia (HI) initially suppresses cerebral oxygen metabolism, but sparks a rapid rebound and overshoot of post-HI $CMRO_2$ caused by uncoupled OXPHOS with greater ROS emission, which leads to the demise of mitochondria and the onset of secondary energy failure (SEF). In contrast, recovery at hypothermia attenuates the post-HI surge of mitochondrial respiration and produces more enduring cerebral oxygen metabolism. The threshold of $CMRO_2$-reduction that causes brain infarction in neonates is expected to exist but yet to be established. (**B**) The combination of energy deficit and tissue acidosis accumulated during HI plus increased glucose-uptake and glycolysis acutely after HI stimulates uncoupled OPXHOS in the HI-injured neonatal brain, leading to excessive ROS emission and rapid mitochondrial injury. According to the literature (Berntman et al., 1981; Hägerdal et al., 1975) and our results, hypothermia may interrupt this pathological process by inhibiting glycolysis and the TCA cycle.

the post-HI brain. Previous studies showed that mild hypothermia represses glycolysis and the tricarboxylic acid (TCA) cycle at the phosphofructokinase and isocitrate dehydrogenase step, respectively (Berntman et al., 1981; Hägerdal et al., 1975). Consequently, the buildup of lactate and acidosis and the electron transport chain reactions in OXPHOS are attenuated, which may repress post-HI mitochondrial respiration and prevent SEF and brain injury according to our hypothesis (Figure 5B).

Whether hypothermia reduces post-HI brain glucose-uptake, however, remains unclear. Although previous studies showed a reverse correlation of cerebral glucose metabolism (CMRglu) and the severity of HIE in neonates at 4–24 days of age (Thorngren-Jerneck et al., 2001), the responses of CMRglu in the acute post-HI phase remain unknown. If post-HI CMRglu is similarly up-regulated due to energy deficit, the influx of glucose and the ensuing glycolysis may stimulate mitochondrial respiration to produce greater ROS injury, while hypothermia typically represses CMRglu and could reduce HI injury in this scenario (Erecinska et al., 2003). Future studies are thus warranted to examine the impacts of HI with or without hypothermia treatment on CMRglu in mouse neonates.

## Optical $CMRO_2$ detection in neonatal care

Early detection of brain injury in neonatal care has profound importance for early intervention, treatment optimization, and outcome prognostication. Although MRI is the gold standard for detecting acute brain injury, its application in early diagnosis and HIE therapy is hampered by non-portability, high cost, and susceptibility to motion. In contrast, advances in combined near infrared spectroscopy (NIRS) and diffuse correlation spectroscopy (DCS) have enabled optical $CMRO_2$ detection as a non-invasive, bedside procedure in neonatal care (De Carli et al., 2019; Dehaes et al., 2014; Ferradal et al., 2017; Jain et al., 2014; Liu et al., 2014a). This is owing to the relatively thin infant skull compared to that of adults and the separation of anterior and posterior fontanelle sutures, which facilitate the penetration of infrared light to quantify the brain tissue oxygenation. The combination of NIRS-based cerebral oximetry and DCS-based CBF mapping in the same area enables quantitative measurements of the regional $CMRO_2$ index or $CMRO_{2i}$. The NIRS/DCS-measured $CMRO_{2i}$ correlates well with the MRI-measured $CMRO_2$ in neonates and declines during hypothermic cardiopulmonary bypass (Dehaes et al., 2014; Ferradal et al., 2017; Jain et al., 2014). A phase 1 clinical trial (NCT02815618) is underway to determine the safety of NIRS/DCS and the normal $CMRO_{2i}$ in newborn infants (De Carli et al., 2019). Notably, our PAM technique is analogous to NIR/DCS, and both methods measure $CMRO_2$ in the cortical layers. Moreover, a past NIR/DCS study suggested increased cerebral oxygen consumption in infants with HIE symptoms (Grant et al., 2009), which echoes our findings. Thus, our results may shed insights into the utility of optical $CMRO_2$ detection in neonatal care. Additionally, the spatial heterogeneity in estimated $CMRO_2$ observed in our data may reflect underlying physiological variability, including differences in vascular structure or metabolic demand across cortical regions. Future studies will aim to further validate and interpret these spatial patterns.

In adult ischemic stroke patients, $CMRO_2$ can be used to differentiate the infarct core and the adjacent penumbra area, where brain cells are energy-strained but remain salvageable if local blood oxygen supply is restored promptly (Lin and Powers, 2018). The cut-off for “salvageable penumbra” is usually at <60% reduction of $CMRO_2$ (Lee et al., 2003). Our results showed that HI-injured mouse neonates preserved 85% of $CMRO_2$ at 24 hours post-HI if recovered under mild hypothermia (32 °C), but lost ~75% of $CMRO_2$ without this treatment (Figure 4G). Further, the severity of $CMRO_2$-reduction at 24 hours correlate with infarction, as shown by the results of TTC-stain immediately after PAM-imaging (Figure 4B and C). These results suggest that a minimal level of $CMRO_2$ to prevent infarction may also exist in infants after HI, as in adults after ischemic stroke, despite that the normal $CMRO_2$ in infants is lower than that in adults and may differ between term and preterm neonates (Altman et al., 1993; Liu et al., 2014b). Since NIRS/DCS-

based $CMRO_{2i}$ measurement is a non-invasive procedure, it can be performed repeatedly to detect early brain injury through the trajectory of $CMRO_{2i}$ alterations in neonates with clinical HIE symptoms.

### Limitations in this study

While P10 mice are widely used to model near-term human infants, developmental differences in cellular metabolism and neurovascular coupling may affect the observed outcomes and limit direct clinical translation (Clancy et al., 2007; Mallard and Vexler, 2015; Sheldon et al., 2018). Nevertheless, the P10 model remains a valuable and widely accepted tool for studying neonatal hypoxia-ischemia mechanisms and evaluating therapeutic interventions.

A technical limitation is the absence of direct intracortical temperature measurements during hypothermia; we relied on skull temperature, which may not fully capture temperature dynamics in deeper cortical layers. However, this approach aligns with clinical practice, where intracortical temperature is not typically measured. Future studies could benefit from more precise intracortical assessments. Another limitation of this study is the restricted imaging depth of the PAM technique, which is typically less than 1 mm and therefore does not allow assessment of deeper brain structures such as the basal ganglia. Yet, in experimental models and clinical cases of neonatal hypoxia-ischemia, the cortical injury tends to be more prominent and functionally significant. As such, our results remain relevant for investigating the pathological mechanisms and therapies of this neonatal brain disorder.

While our study focuses on the acute effects of hypothermia, previous research has shown long-term neuroprotective benefits, including improved white matter development post-injury (Koo et al., 2017). These findings highlight the potential of hypothermia for both immediate and extended recovery, warranting further study of long-term outcomes.

Lastly, for awake imaging, the small size of neonatal mice at P10 aids stability during awake PAM imaging, though it limits the feasibility of prior training, which is typically possible in older animals. We observed no signs of distress or pain and did not use stress- or pain-reducing drugs during imaging. However, potential effects of stress or residual pain on CBF and $CMRO_2$ cannot be fully ruled out. Future studies could incorporate more detailed pain assessment and stress-mitigation strategies to further enhance physiological reliability.

## Methods

### Multi-parametric PAM System

As shown in Figure 1A, a nanosecond-pulsed laser (wavelength: 532 nm, repetition rate: up to 30 kHz; BX40-2-G, EdgeWave) was used in the PAM system for imaging the neonatal mouse brain. The laser beam firstly passed through a half-wave plate (HWP; WPH05M-532, Thorlabs) and an electro-optical modulator (EOM; 350-80, Conoptics) for precise control of the polarization state of the incident beam. By alteration of the voltage applied to the EOM, the polarization state could be dynamically switched between the vertical direction and the horizontal direction, which allowed a polarizing beam splitter (PBS; PBS121, Thorlabs) to dispatch the laser pulses between two optical paths through either reflection or transmission. In the reflection path, after being partially attenuated by a neutral-density filter (NDF; NDC-50C-2M, Thorlabs), the beam was coupled through a fiber collimator (CFC-11X-A, Thorlabs) into a polarization-maintaining single-mode fiber (PM-SMF; F-SPA, Newport) for stimulated Raman scattering-based wavelength conversion. The output of the PM-SMF was collimated by an identical collimator and purified by a bandpass filter (BPF; FB560-10, Thorlabs) to isolate the 558-nm component. Then, the 558-nm Raman beam generated in the reflection path and the 532-nm beam in the transmission path were combined by a dichroic mirror (DBS; FF538-FDi01, Semrock) and coupled into a single-mode fiber (SMF; P1-460B-FC-2, Thorlabs) through a fiber collimator (CFC-11X-A, Thorlabs), before which ~5% of the combined beam was picked off by a beam sampler (BS; BSF10-A, Thorlabs) and monitored by a high-speed photodiode (PD; FDS100, Thorlabs) to compensate for possible fluctuation in the laser energy. The dual-wavelength laser beam was then delivered to the scanning head, where two

identical doublets (DL; AC127-025-A, Thorlabs) were used to map the fiber output into the tissue to be imaged, and a correction lens (CL; LA1207-A, Thorlabs) was used to compensate for the optical aberration at the air-water interface. A ring-shaped ultrasonic transducer (UT; inner diameter: 2.2 mm; outer diameter: 4.0 mm; center frequency: 35 MHz; 6-dB bandwidth: 70%) was used for confocal alignment of the optical excitation and ultrasonic detection. A customized water tank (WT) was used to immerse the ultrasonic transducer for acoustic coupling. As shown in Figure 1B, the mouse head was fixed to a customized metal arm-piece through a wearable 3-D printed head plate for head-restrained awake-brain imaging. A water-floated treadmill (03170-1008, Blick Art Materials) was used to allow the mouse to move freely with reduced reaction force (Cao et al., 2017). A gas inlet and a customized face mask from syringe were used to deliver the inhalation gas (*i.e.,* normoxia or hypoxia).

## Procedures for PAM Imaging

Before imaging of the neonatal mouse brain, the animal was first anesthetized with vaporized isoflurane (EZ-SA800, E-Z Systems) for installation of the head-restraint plastic head plate (Sciortino et al., 2021). To manage pain, 0.25% Bupivacaine was administered locally prior to the surgical procedures. Hair on the mouse scalp was removed by a trimmer (9990-1301, Wahl Clipper), and then the scalp was removed with surgical scissors (MDS10030, Medline Industries) to expose the skull. After the clearance of the blood, debris, and remaining hairs, the gel-based cyanoacrylate glue (234790, Loctite) was applied to all edges of the head plate, which was attached to the center of the skull between the Bregma and Lambda. After the applied glue is solidified (~20 min), the frame-worn animal was first returned to its cage for full recovery from anesthesia, and then carefully moved to the treadmill and secured to the metal arm-piece with two #4–40 screws for awake PAM imaging. The total duration of anesthesia, including preparation and glue solidification, was approximately 20 minutes. Throughout the frame installation, the body temperature of the mouse was maintained at 37 °C using a homeothermic monitoring system (No. 69020, RWD life science).

After the installation of the head-restraint head plate, a thin layer (~1 mm) of ultrasound gel (Aquasonic CLEAR®, Parker Laboratories) was applied to the surface of the skull for effective acoustic coupling. Then, the metal arm-piece and the treadmill were carefully raised to bring the gel in gentle contact with the bottom of the water tank, which was filled with temperature-maintained deionized water. After fully recovering from the anesthesia, the neonatal mouse was ready for awake-brain imaging by the multi-parametric PAM system, which was controlled by a field-programmable gate array (PCIe-7841R, National Instruments) through a self-developed LabVIEW program. For the imaging field covering both hemicortices between the Bregma and Lambda of the neonatal mouse (5 × 3 $mm^2$ as shown in Figure 1C, with each hemicortex measuring 2.5 × 3 $mm^2$), the acquisition time is ~40 minutes with step sizes set to 0.1 and 10 μm along the *x*- and *y*-direction, respectively.

## PAM Imaging under Normothermia or Hypothermia

The temperature of the water tank was controlled by a temperature controller (EW-89802-52, Cole-Parmer), which could also be used to effectively regulate the temperature of the underlying mouse skull. Based on our calibration experiment (Figure S1), the normothermia condition (37 °C) could be achieved with the water temperature set to 39 °C; while for the two hypothermia conditions (32 °C or 29 °C), the water temperature was set to 33 °C or 29 °C, respectively. Throughout all the experiments, the skull temperature was closely monitored by a thin-film temperature sensor (F3132, Omega) attached to the skull. Note that the PAM measurements were performed one hour after each temperature adjustment to ensure equilibrium under the new temperature setting.

## PAM Imaging under Normoxia or Hypoxia

For normoxia, the oxygen concentration in the inhalation gas was 21% (AI M-T, Praxair). For hypoxia, the medical-grade air was mixed with medical-grade nitrogen gas (NI-H, Praxair) through a gas flowmeter mixer (EW-03218-56, Cole-Parmer) to achieve a reduced oxygen concentration of 10%, which was confirmed by a clinical anesthesia monitor (Capnomac Ultima, Datex-Ohmeda). Under both conditions, the flow rate of the inhalation gas was set to 1.5 L/min.

## PAM Imaging of the Vannucci HI Model

In the Vannucci HI study, the first PAM image set was acquired at 37 °C after the unilateral CCA ligation. Then, the second image set was acquired at 37 °C during the one-hour HI challenge. Subsequently, three sequential image sets were acquired up to 120 minutes (*i.e.*, 0–40, 40–80, and 80–120 minutes) post-HI, either under normothermia (37 °C) or hypothermia (32 °C) by regulating the temperature of the water tank.

## Quantification of Cerebral Hemodynamics and Oxygen Metabolism by PAM

Our PAM technique enables simultaneous quantification of multiple microvascular parameters, including $C_{Hb}$, $sO_2$, and blood flow by the statistical, spectroscopic, and correlation analyses of the acquired A-line signals, respectively (Cao et al., 2017). With our self-developed MATLAB-based vessel segmentation algorithm (Sun et al., 2020), these hemodynamic parameters could be extracted at the single-microvessel level. Briefly, this process involves generating a vascular map using signal amplitude obtained from the Hilbert transformation, selecting a region slightly larger than the vessel of interest, and applying Otsu's thresholding method to remove background pixels. Isolated or spurious boundary fragments are then removed to improve boundary smoothness. The customized MATLAB code used for vessel segmentation is available upon request. Then, CBF, OEF, and $CMRO_2$ could be obtained by the following formulas:

$$CBF = \pi v d^2/8$$

$$OEF = (s_aO_2 - s_vO_2)/s_aO_2$$

$$CMRO_2 = \xi \times C_{Hb} \times s_aO_2 \times OEF \times CBF$$

where $d$ is the vascular diameter, $v$ is the peak flow speed along the vascular axis, $s_aO_2$ and $s_VO_2$ are the $sO_2$ values of the feeding arteries and draining veins, respectively (Cao et al., 2017), and $\xi$ is the oxygen binding capacity of hemoglobin (0.014 L $O_2$ per gram hemoglobin).

## Neonatal Cerebral HI and Hypothermia Treatment

The Vannucci model of neonatal HI with and without hypothermia treatment was performed in P10 C57BL/6 mice as described (Chen et al., 2021; Kuan et al., 2021; Yang et al., 2009). P10 mice were chosen for our experiments as they are widely used to model near-term infants in humans. At this developmental stage, the brain maturation in mice closely parallels that of near-term infants, making them an appropriate model for studying neonatal brain injury and therapeutic interventions (Clancy et al., 2007; Mallard and Vexler, 2015; Sheldon et al., 2018). Briefly, P10 mice of both sexes anesthetized with 2% isoflurane were subjected to the right CCA-ligation. To manage pain, 0.25% Bupivacaine was administered locally prior to the surgical procedures, which took less than 10 minutes. After a recovery period for one hour, awake mice were exposed to 10% $O_2$ for 40 minutes in a hypoxic chamber at 37 °C. The mice were recovered to normoxia (21% $O_2$) condition, and then randomly divided into normothermia or hypothermia groups with the chambers submerged in a 37 °C or 32 °C water bath, separately for a total four-hour treatment. The body temperature of mice was monitored at 37 °C or 32 °C using a rectal probe (BAT-12 microprobe, Physitemp) during the treatment.

## Measurement of Brain Infarction

Detection of brain infarction was performed by TTC staining (Sigma-Aldrich) at 24 hours post-HI as previously described (Kuan et al., 2021; Yang et al., 2009). The fresh brains were collected after cold-PBS transcardial perfusion. The whole brain (Figure 4C) or 1 mm-thick brain sections (Figure 4D) were incubated with 2% TTC solution, and the TTC-unstained volume in all sections were quantified using the NIH ImageJ software.

## HR-MAS NMR Study

The *ex-vivo* NMR experiments and analyses of mice brain tissues were performed as previously reported (Chen et al., 2021). Briefly, a 1.5-mm punch (~10 mg) was taken from snap-frozen brain tissue and loaded into a sample rotor (4 mm $ZrO_2$, Bruker Instruments), with 4 μL of deuterium oxide containing 100 mM sodium trimethylsilylpropionate-d4 (TSP, Sigma-Aldrich) added to obtain a frequency-lock signal and serve as an internal standard for chemical shift. HR-MAS NMR experiments were then carried out on an NMR spectrometer (AVANCE 400 WB, Bruker) with a dedicated 4 mm HR-MAS probe. Spinning rate of samples was set to 2500 kHz (± 2 Hz) at 4 °C. A T2-weighted, water-suppressed Carr-Purcell-Meiboom-Gill pulse sequence was used to acquire the data. The $^1$H-NMR spectra were recorded using key parameters as follows: repetition time of 2.0 seconds, spectral width of 4.8 kHz, 32K data points, and 256 transients. The presence and concentrations of selected metabolites in brain tissue samples were determined based on their chemical shifts and corresponding integrals using the Electronic REference To access In vivo Concentration (ERETIC) reference method (Bruker), with 10 mM TSP as the external standard.

## ATP Detection

The brain ATP level was measured through an ATP Assay Kit (Catalog No. ab83355, Abcam) according to the manufacturer's instructions. Briefly, mouse brains were harvested, washed with 1X PBS, and then resuspended in 100 μL of ATP assay buffer. Cells were homogenized and then centrifuged at 4 °C at 12,000 g to remove the insoluble material. The supernatants were collected and incubated with the ATP probe. Absorbance was detected at 580 nm using a microplate reader (SpectraMax® M3 Microplate Reader, Molecular Devices).

## Assessment of Isolated Brain Mitochondrial Function

Mitochondria were isolated from the brain tissues using Percoll density gradient centrifugation as described before (Caspersen et al., 2008; Niatsetskaya et al., 2012). Mitochondrial respiration was measured by a Clark-type electrode (Oxytherm, Hansatech). Briefly, 0.05 mg mitochondria protein were added into 0.5 mL respiration buffer at pH 7.2, which consists of 200 mM sucrose, 25 mM KCl, 2 mM $K_2HPO_4$, 5 mM HEPES, 5 mM $MgCl_2$, 0.2 mg/mL of BSA, 30 μM $P^1$, $P^5$-di(adenosine 5')-pentaphosphate (Ap5A), 10 mM glutamate, and 5 mM malate at 32°C, with the addition of 5 mM succinate to trigger respiration. As shown in Figure S2, to initiate State 3 phosphorylating respiration, 100 nmol of adenosine diphosphate (ADP) was added to the mitochondrial suspension.

The rate of $O_2$ consumption was presented in nmol $O_2$/mg mitochondrial protein/min. The respiratory control ratio was calculated as the ratio of the State 3 respiration rate versus the State 4 resting respiration rate recorded after the phosphorylation of ADP has been finished. 35 nM 2'-4' Dinitrophenol (DNP) was used to initiate uncoupled respiration (Kim et al., 2018).

The rate of $H_2O_2$ emission from isolated mitochondria was measured using a fluorescence assay by a fluorescence spectrophotometer (F-7000, Hitachi High Technologies America, Inc), which was set at 555-nm excitation and 581-nm emission as previous study (Starkov and Fiskum, 2003). Briefly, 0.05 mg mitochondria were added into 1 mL respiration buffer and supplemented with 5 mM succinate, 10 μM Amplex Ultrared (Catalog No. A22180, Invitrogen), and 4 U/mL horse radish peroxidase (HRP). After recording the fluorescence for 400 seconds, samples were added with 1 μM rotenone, then added with 1μg/mL antimycin A after another 200 seconds. The calibration curve was calculated by sequential additions of known amounts of $H_2O_2$, with the cuvette containing the respiration buffer, Amplex Ultrared, and HRP.

Superoxide was monitored with MitoSOX Red (Catalog No. M36008, Invitrogen). Briefly, 5 μM MitoSOX Red was added to the cuvettes and the fluorescence was measured at 510-nm excitation and 579-nm emission wavelengths. Time-dependent monitoring of the MitoSOX Red-related fluorescence was done using a fluorescence spectrophotometer (F-7000, Hitachi High Technologies America, Inc) at 25 °C. Since a saturation of kinetics established after 25 minutes of the recording, the initial linear increase rates of the MitoSOX Red-related fluorescence were used for quantification.

For membrane potential analysis, the rhodamine 123 (RH-123; Sigma-Aldrich) quenching technique was conducted. 0.05 mg isolated mitochondria were incubated with 0.3 mM RH-123 and analyzed by a fluorescence spectrophotometer (F-7000, Hitachi High Technologies America, Inc), using excitation and emission wavelengths of 503 nm and 527 nm, respectively. During the measurements, the reaction buffer containing mitochondria was continuously stirred. Baseline fluorescence was recorded for 300 seconds followed by the sequential addition of oxidizable substrates (7 mM succinate or 7 mM malate and glutamate) and 50 mM carbonyl cyanide m-chlorophenyl hydrazone (CCCP).

### Video-EEG Monitoring

Video-EEG monitoring of mouse neonates was performed as described (Burnsed et al., 2019). Briefly, nine-day-old C57BL/6 mice had unipolar insulated stainless steel depth electrodes (bare diameter: 0.005 inch, coated: 0.008 inch; A-M Systems, Sequim) stereotactically implanted in the bilateral parietal cortices (−1.2 dorsoventral (DV), ±0.5 mediolateral (ML), and −1.0 deep (D) mm), bilateral CA1 region of the hippocampus (−3.5 DV, ±2.0 ML, and −1.75 D mm), and a reference electrode in the cerebellum. Following recovery, mice were exposed to HI on P10. A unity gain impedance matching head stage (TLC2274 Quad Low-Noise Rail-to Rail Operational Amplifier, Texas Instruments) was used for recordings, which began 1 hour prior to CCA ligation and continued through 2 hours after re-oxygenation post-ligation. Mice were then returned to the dam.

### Statistical Analysis

One-way ANOVA was used to compare the vascular and oxygen-metabolic changes in the normothermia *vs.* hypothermia experiment (Figure 1E), and to assess mitochondrial function in the UN, CL, and IL cortices (Figure 2F–H). Student t-test was used to compare the hemodynamic and oxygen-metabolic changes in the normoxia *vs.* hypoxia experiment (Figure 1G), and the infarct volume of normothermia or hypothermia (Figure 4D). Two-way ANOVA was used to compare the oxygen-metabolic changes of the CL and IL cortices in the Vannucci HI model under normothermic (Figure 2B–D) or hypothermic (Figure 3B–E) condition, the mitochondrial function (Figure 3F–I) and ATP level (Figure 3J) of CL or IL cortices under hypothermia, and the hemodynamic and oxygen-metabolic changes 24 hours post-HI (Figure 4E–I). All data were presented in the form of mean ± standard deviation of the mean. In all statistical analyses, $p < 0.05$ was considered significant.

## Data availability

All data generated or analyzed during this study are included in the manuscript and supporting files; source data files are available upon request.

## Supplementary files

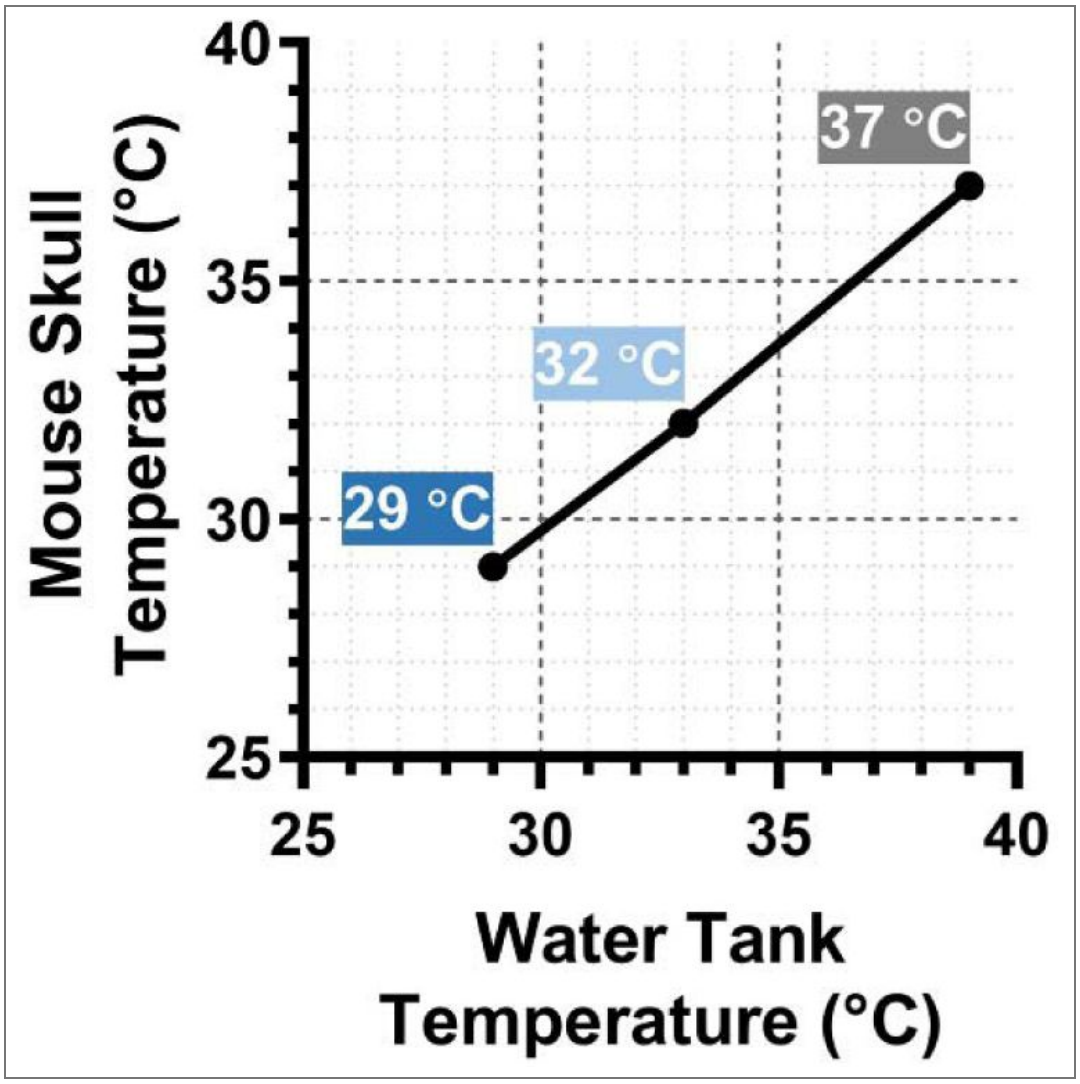


**Figure S1.** **Relationship between the water tank temperature and the mouse skull temperature.**

**Figure S2. Oxygen consumption of mitochondria isolated from the uninjured (UN), contralateral (CL), and ipsilateral (IL) cortex at (*A*) 2 hours or (*B*) 5 hours post-HI.**

HI, hypoxia-ischemia; mito, mitochondria protein; ADP, adenosine diphosphate; DNP, 2'-4' Dinitrophenol; OCR, oxygen consumption rate.

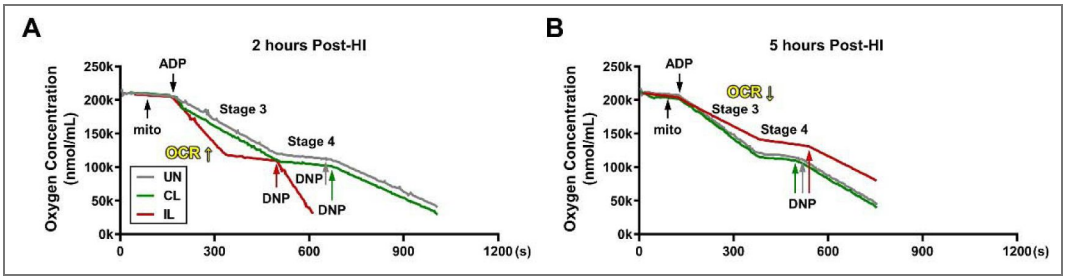


**Figure S3. 1H-HRMAS MRS analysis of the effects of normothermia *vs.* hypothermia on brain metabolites at 24 hours post-HI. NAA, N-acetyl aspartate; Cr, creatine; PCr, phosphocreatine; Cho, choline; Glx, glutamate.**

Two-way ANOVA was performed (nD=D5 for normothermia and n = 3 for hypothermia). *, *p*D<D0.05; **, *p*D<D0.01.

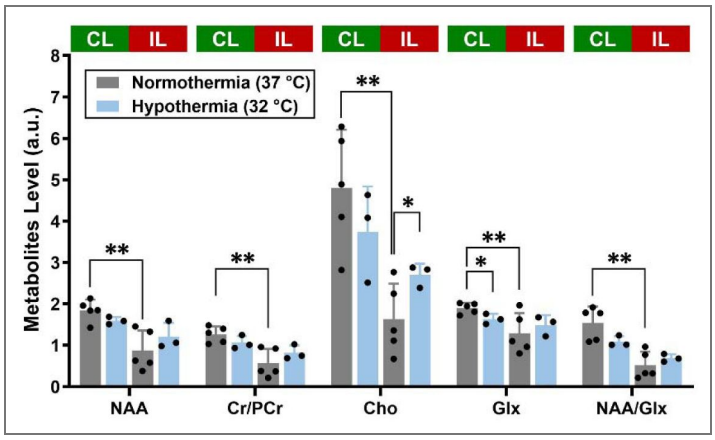


**Figure S4. Potential mechanisms that contribute to the uncoupling of OXPHOS after HI and the effects of therapeutic hypothermia.**

OMM, outer mitochondrial membrane; IMM, inner mitochondrial membrane; IMS, mitochondrial intermembrane space; ROS, reactive oxygen species; NADH nicotinamide adenine dinucleotide hydrogen; $FADH_2$, flavin adenine dinucleotide; CoQ, Coenzyme Q; cyt c, cytochrome complex; NO, nitric oxide; CCO, cytochrome c oxidase; $\Delta\Psi_m$, mitochondrial membrane potential; MCU, mitochondrial calcium uniporter; OXPHOS, oxidative phosphorylation.

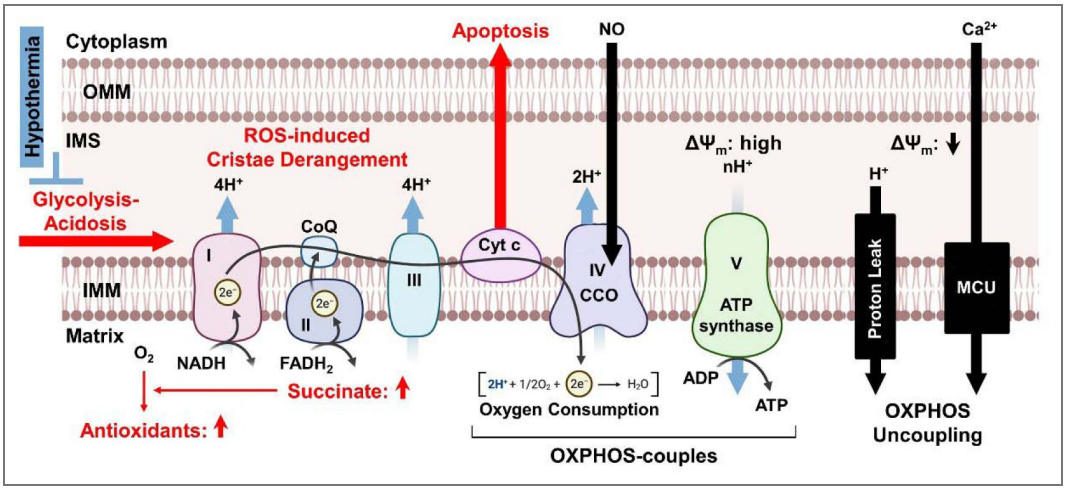

**Table S1.** **CBF, OEF, and $CMRO_2$ values measured at 37 °C in the contralateral (green) and ipsilateral (red) cortex in the indicated period that correspond to those illustrated in Fig. 2A.**

Data are shown in mean ± SD and compared to the "CCA-ligation" on its own side, unless indicated with a bracket. The *p*-values were determined by two-way ANOVA (n=5; *: p<0.05; **: p<0.01).

| Normothermia (37 °C) | Contralateral (CL) Hemisphere | | | |
|---|---|---|---|---|
| | CBF (mL/100g/min) | OEF | $CMRO_2$ (mL/100g/min) | |
| CCA-ligation | 26.67 ± 2.86 | 0.21 ± 0.05 | 1.26 ± 0.25 | |
| Hypoxia-Ischemia | 35.11 ± 1.87 | 0.44 ± 0.03 | 2.37 ± 0.36 | ** |
| Post-HI (0–40 mins) | 36.92 ± 3.88 | 0.22 ± 0.07 | 1.80 ± 0.63 | |
| Post-HI (40–80 mins) | 39.14 ± 4.53 | 0.23 ± 0.06 | 1.96 ± 0.55 | * |
| Post-HI (80–120 mins) | 41.85 ± 2.64 | 0.25 ± 0.09 | 2.28 ± 0.73 | ** |
| Normothermia (37 °C) | Ipsilateral (CL) Hemisphere | | | |
| | CBF (mL/100g/min) | OEF | $CMRO_2$ (mL/100g/min) | |
| CCA-ligation | 23.67 ± 5.21 | 0.30 ± 0.05 | 1.56 ± 0.31 | |
| Hypoxia-Ischemia | 26.03 ± 3.43 | 0.25 ± 0.08 | 0.78 ± 0.18 | * |
| Post-HI (0–40 mins) | 28.31 ± 3.10 | 0.38 ± 0.12 | 2.30 ± 0.63 | * |
| Post-HI (40–80 mins) | 29.79 ± 5.32 | 0.36 ± 0.09 | 2.34 ± 0.68 | * |
| Post-HI (80–120 mins) | 30.48 ± 3.59 | 0.34 ± 0.07 | 2.39 ± 0.42 | * |

**Table S2.** **CBF, OEF, and $CMRO_2$ values with post-HI hypothermia treatment, measured at 32 °C in the contralateral (green) and ipsilateral (red) cortex in the indicated period that correspond to those illustrated in Fig. 3A.**

Data are shown in mean ± SD and compared to the "CCA-ligation" on its own side, unless indicated with a bracket. The *p*-values were determined by two-way ANOVA (n=5; ***: p<0.001; ****: p<0.0001).

| Hypothermia (32 °C) | Contralateral (CL) Hemisphere | | | |
|---|---|---|---|---|
| | CBF (mL/100g/min) | OEF | $CMRO_2$ (mL/100g/min) | |
| CCA-ligation | 26.18 ± 3.06 | 0.23 ± 0.02 | 1.56 ± 0.41 | |
| Hypoxia-Ischemia | 31.23 ± 4.96 | 0.42 ± 0.06 | 2.46 ± 0.49 | **** |
| Post-HI (0–40 mins) | 36.06 ± 5.64 | 0.22 ± 0.02 | 1.64 ± 0.30 | |
| Post-HI (40–80 mins) | 37.32 ± 2.75 | 0.21 ± 0.04 | 1.78 ± 0.16 | |
| Post-HI (80–120 mins) | 38.97 ± 2.50 | 0.21 ± 0.05 | 1.62 ± 0.29 | |
| Hypothermia (32 °C) | Ipsilateral (CL) Hemisphere | | | |
| | CBF (mL/100g/min) | OEF | $CMRO_2$ (mL/100g/min) | |
| CCA-ligation | 24.61 ± 1.75 | 0.25 ± 0.02 | 1.55 ± 0.44 | |
| Hypoxia-Ischemia | 28.13 ± 6.78 | 0.28 ± 0.05 | 0.90 ± 0.44 | *** |
| Post-HI (0–40 mins) | 29.89 ± 4.46 | 0.25 ± 0.04 | 1.32 ± 0.44 | |
| Post-HI (40–80 mins) | 28.90 ± 3.25 | 0.22 ± 0.02 | 1.38 ± 0.36 | |
| Post-HI (80–120 mins) | 28.84 ± 3.22 | 0.22 ± 0.02 | 1.40 ± 0.38 | |

## Acknowledgements

We thank Dr. Vadim Ten for demonstrating the mitochondria isolation and analysis methods.

## Additional information

### Funding

This work was supported by the National Science and Technology Council of Taiwan MOST 111-2320-B-110-003-MY2 (to Y.-Y.S.), NIH grants NS125788, NS135793, NS127392, and HD109025 (to C.-Y.K.), NS099261 and NS120481 (to S.H.), and NS125677 (to C.-Y.K. and S.H.), and NSF CAREER 202988 (to S.H.).

### Author contributions

S.H. and C.-Y.K. came up the research idea. D.M.L., P.E.G., S.H., and C.-Y.K. finalized the research plan and interpreted the experimental data. N.S., Y.-Y.S., R.C., H.-R.C., Y.W., E.F., M.R.S., and Y.-M.K. performed the experiment. S.H. and C.-Y.K. wrote the manuscript.

### Ethics

All procedures were approved by the Institutional Animal Care and Use Committees at the University of Virginia and Washington University in St. Louis.

### List of Abbreviations

ATP: adenosine triphosphate
CBF: cerebral blood flow
CCA: common carotid artery
CCO: cytochrome c oxidase
CHb: total concentration of hemoglobin
Cho: choline
CL: contralateral
CMRglu: cerebral glucose metabolism
CMRO2: cerebral metabolic rate of oxygen
Cr/PCr: total creatine/ phosphocreatine
DCS: diffuse correlation spectroscopy
EEG: electroencephalography
EOM: electro-optical modulator
Glx: glutamate and glutamine
HI: hypoxia-ischemia
HIE: hypoxic-ischemic encephalopathy
IL: ipsilateral
MRI: magnetic resonance imaging
NIRS: near infrared spectroscopy
NMR: nuclear magnetic resonance
OCR: oxygen consumption rate
OEF: oxygen extraction fraction
OXPHOS: oxidative phosphorylation
P10: postnatal 10-day-old
PAM: photoacoustic microscopy
PET: positron emission tomography
ROS: reactive oxygen species
SEF: secondary energy failure
sO2: saturation of hemoglobin
TTC: tetrazolium chloride
UN: uninjured

## Funding

| Funder | Grant reference number | Author |
|---|---|---|
| National Science and Technology Council | MOST 111-2320-B-110-003-MY2 | Yu-Yo Sun |
| National Institutes of Health | NS125788 | Chia-Yi Kuan |
| National Institutes of Health | NS135793 | Chia-Yi Kuan |
| National Institutes of Health | NS127392 | Chia-Yi Kuan |
| National Institutes of Health | HD109025 | Chia-Yi Kuan |
| National Institutes of Health | NS099261 | Song Hu |
| National Institutes of Health | NS120481 | Song Hu |
| National Institutes of Health | NS125677 | Song Hu<br>Chia-Yi Kuan |
| National Science Foundation | NSF CAREER 202988 | Song Hu |

## Author ORCID iDs

**P Ellen Grant**: http://orcid.org/0000-0003-1005-4013

# References

**Allen KA,** Brandon DH (2011) Hypoxic Ischemic Encephalopathy: Pathophysiology and Experimental Treatments. *Newborn Infant Nurs Rev* **11**:125-133 https://doi.org/10.1053/j.nainr.2011.07.004

**Altman DI,** Perlman JM, Volpe JJ, Powers WJ (1993) Cerebral oxygen metabolism in newborns. *Pediatrics* **92**:99-104

**Benzi RH,** Lerch R (1992) Dissociation between contractile function and oxidative metabolism in postischemic myocardium. Attenuation by ruthenium red administered during reperfusion. *Circ Res* **71**:567-576 https://doi.org/10.1161/01.res.71.3.567

**Berntman L,** Welsh FA, Harp JR (1981) Cerebral protective effect of low-grade hypothermia. *Anesthesiology* **55**:495-498 https://doi.org/10.1097/00000542-198111000-00003

**Blumberg RM,** Cady EB, Wigglesworth JS, McKenzie JE, Edwards AD (1997) Relation between delayed impairment of cerebral energy metabolism and infarction following transient focal hypoxia-ischaemia in the developing brain. *Exp Brain Res* **113**:130-137 https://doi.org/10.1007/BF02454148

**Buckley EM,** Patel SD, Miller BF, Franceschini MA, Vannucci SJ (2015) In vivo Monitoring of Cerebral Hemodynamics in the Immature Rat: Effects of Hypoxia-Ischemia and Hypothermia. *Dev Neurosci* **37**:407-416 https://doi.org/10.1159/000381704

**Burnsed J,** Skwarzyńska D, Wagley PK, Isbell L, Kapur J (2019) Neuronal Circuit Activity during Neonatal Hypoxic-Ischemic Seizures in Mice. *Ann Neurol* **86**:927-938 https://doi.org/10.1002/ana.25601

**Cao R,** Li J, Ning B, Sun N, Wang T, Zuo Z, Hu S (2017) Functional and oxygen-metabolic photoacoustic microscopy of the awake mouse brain. *NeuroImage* **150**:77-87 https://doi.org/10.1016/j.neuroimage.2017.01.049

**Caspersen CS,** Sosunov A, Utkina-Sosunova I, Ratner VI, Starkov AA, Ten VS (2008) An isolation method for assessment of brain mitochondria function in neonatal mice with hypoxic-ischemic brain injury. *Dev Neurosci* **30**:319-324 https://doi.org/10.1159/000121416

**Chen H-R,** DeGrauw T, Kuan C-Y (2022) (Phospho)creatine: the reserve and merry-go-round of brain energetics. *Neural Regen Res* **18**:327-328 https://doi.org/10.4103/1673-5374.346470

**Chen H-R,** Zhang-Brotzge X, Morozov YM, Li Y, Wang S, Zhang HH, Kuan IS, Fugate EM, Mao H, Sun Y-Y, *et al.* (2021) Creatine transporter deficiency impairs stress adaptation and brain energetics homeostasis. *JCI Insight* **6**:140173 https://doi.org/10.1172/jci.insight.140173

**Clancy B,** Kersh B, Hyde J, Darlington RB, Anand KJS, Finlay BL (2007) Web-based method for translating neurodevelopment from laboratory species to humans. *Neuroinformatics* **5**:79-94 https://doi.org/10.1385/ni:5:1:79

**Cooper CE,** Giulivi C (2007) Nitric oxide regulation of mitochondrial oxygen consumption II: Molecular mechanism and tissue physiology. *Am J Physiol Cell Physiol* **292**:C1993-2003 https://doi.org/10.1152/ajpcell.00310.2006

**De Carli A,** Andresen B, Giovannella M, Durduran T, Contini D, Spinelli L, Weigel UM, Passera S, Pesenti N, Mosca F, *et al.* (2019) Cerebral oxygenation and blood flow in term infants during postnatal transition: BabyLux project. *Arch Dis Child Fetal Neonatal Ed* **104**:F648-F653 https://doi.org/10.1136/archdischild-2018-316400

**Dehaes M,** Aggarwal A, Lin P-Y, Rosa Fortuno C, Fenoglio A, Roche-Labarbe N, Soul JS, Franceschini MA, Grant PE (2014) Cerebral oxygen metabolism in neonatal hypoxic ischemic encephalopathy during and after therapeutic hypothermia. *J Cereb Blood Flow Metab* **34**:87-94 https://doi.org/10.1038/jcbfm.2013.165

**Erecinska M,** Thoresen M, Silver IA (2003) Effects of hypothermia on energy metabolism in Mammalian central nervous system. *J Cereb Blood Flow Metab* **23**:513-530 https://doi.org/10.1097/01.WCB.0000066287.21705.21

**Ferradal SL,** Yuki K, Vyas R, Ha CG, Yi F, Stopp C, Wypij D, Cheng HH, Newburger JW, Kaza AK, *et al.* (2017) Non-invasive Assessment of Cerebral Blood Flow and Oxygen Metabolism in Neonates during Hypothermic Cardiopulmonary Bypass: Feasibility and Clinical Implications. *Sci Rep* **7**:44117 https://doi.org/10.1038/srep44117

**Fox PT,** Raichle ME (1986) Focal physiological uncoupling of cerebral blood flow and oxidative metabolism during somatosensory stimulation in human subjects. *Proc Natl Acad Sci U S A* **83**:1140-1144 https://doi.org/10.1073/pnas.83.4.1140

**Gao Y-R,** Ma Y, Zhang Q, Winder AT, Liang Z, Antinori L, Drew PJ, Zhang N (2017) Time to wake up: Studying neurovascular coupling and brain-wide circuit function in the un-anesthetized animal. *Neuroimage* **153**:382-398 https://doi.org/10.1016/j.neuroimage.2016.11.069

**Granger DN,** Kvietys PR (2015) Reperfusion injury and reactive oxygen species: The evolution of a concept. *Redox Biol* **6**:524-551 https://doi.org/10.1016/j.redox.2015.08.020

**Grant PE,** Roche-Labarbe N, Surova A, Themelis G, Selb J, Warren EK, Krishnamoorthy KS, Boas DA, Franceschini MA (2009) Increased cerebral blood volume and oxygen consumption in neonatal brain injury. *J Cereb Blood Flow Metab* **29**:1704-1713 https://doi.org/10.1038/jcbfm.2009.90

**Gunn AJ,** Gunn TR, de Haan HH, Williams CE, Gluckman PD. (1997) Dramatic neuronal rescue with prolonged selective head cooling after ischemia in fetal lambs. *J Clin Invest* **99**:248-256

**Gunn AJ,** Laptook AR, Robertson NJ, Barks JD, Thoresen M, Wassink G, Bennet L (2017) Therapeutic hypothermia translates from ancient history in to practice. *Pediatr Res* **81**:202-209 https://doi.org/10.1038/pr.2016.198

**Hägerdal M,** Harp J, Siesjö BK (1975) Effect of hypothermia upon organic phosphates, glycolytic metabolites, citric acid cycle intermediates and associated amino acids in rat cerebral cortex. *J Neurochem* **24**:743-748

**Jain V,** Buckley EM, Licht DJ, Lynch JM, Schwab PJ, Naim MY, Lavin NA, Nicolson SC, Montenegro LM, Yodh AG, *et al.* (2014) Cerebral oxygen metabolism in neonates with congenital heart disease quantified by MRI and optics. *J Cereb Blood Flow Metab* **34**:380-388 https://doi.org/10.1038/jcbfm.2013.214

**Jespersen SN,** Østergaard L (2012) The roles of cerebral blood flow, capillary transit time heterogeneity, and oxygen tension in brain oxygenation and metabolism. *J Cereb Blood Flow Metab* **32**:264-277 https://doi.org/10.1038/jcbfm.2011.153

**Juhaszova M,** Zorov DB, Kim S-H, Pepe S, Fu Q, Fishbein KW, Ziman BD, Wang S, Ytrehus K, Antos CL, *et al.* (2004) Glycogen synthase kinase-3beta mediates convergence of protection signaling to inhibit the mitochondrial permeability transition pore. *J Clin Invest* **113**:1535-1549 https://doi.org/10.1172/JCI19906

**Khacho M,** Tarabay M, Patten D, Khacho P, MacLaurin JG, Guadagno J, Bergeron R, Cregan SP, Harper M-E, Park DS, *et al.* (2014) Acidosis overrides oxygen deprivation to maintain mitochondrial function and cell survival. *Nat Commun* **5**:3550 https://doi.org/10.1038/ncomms4550

**Kim M,** Stepanova A, Niatsetskaya Z, Sosunov S, Arndt S, Murphy MP, Galkin A, Ten VS (2018) Attenuation of oxidative damage by targeting mitochondrial complex I in neonatal hypoxic-ischemic brain injury. *Free Radic Biol Med* **124**:517-524 https://doi.org/10.1016/j.freeradbiomed.2018.06.040

**Koo E,** Sheldon RA, Lee BS, Vexler ZS, Ferriero DM (2017) Effects of therapeutic hypothermia on white matter injury from murine neonatal hypoxia-ischemia. *Pediatr Res* **82**:518-526 https://doi.org/10.1038/pr.2017.75

**Kramer RS,** Pearlstein RD (1983) Reversible uncoupling of oxidative phosphorylation at low oxygen tension. *Proc Natl Acad Sci U S A* **80**:5807-5811 https://doi.org/10.1073/pnas.80.19.5807

**Kristián T,** Siesjö BK (1998) Calcium in ischemic cell death. *Stroke* **29**:705-718 https://doi.org/10.1161/01.str.29.3.705

**Kuan C-Y,** Chen H-R, Gao N, Kuo Y-M, Chen C-W, Yang D, Kinkaid MM, Hu E, Sun Y-Y (2021) Brain-targeted hypoxia-inducible factor stabilization reduces neonatal hypoxic-ischemic brain injury. *Neurobiol Dis* **148**:105200 https://doi.org/10.1016/j.nbd.2020.105200

**Lally PJ,** Montaldo P, Oliveira V, Soe A, Swamy R, Bassett P, Mendoza J, Atreja G, Kariholu U, Pattnayak S, *et al.* (2019) Magnetic resonance spectroscopy assessment of brain injury after moderate hypothermia in neonatal encephalopathy: a prospective multicentre cohort study. *Lancet Neurol* **18**:35-45 https://doi.org/10.1016/S1474-4422(18)30325-9

**Lee J-M,** Vo KD, An H, Celik A, Lee Y, Hsu CY, Lin W (2003) Magnetic resonance cerebral metabolic rate of oxygen utilization in hyperacute stroke patients. *Ann Neurol* **53**:227-232 https://doi.org/10.1002/ana.10433

**Lin W,** Powers WJ (2018) Oxygen metabolism in acute ischemic stroke. *J Cereb Blood Flow Metab* **38**:1481-1499 https://doi.org/10.1177/0271678X17722095

**Liu P,** Chalak LF, Lu H (2014a) Non-invasive Assessment of Neonatal Brain Oxygen Metabolism: A Review of Newly Available Techniques. *Early Hum Dev* **90**:695-701 https://doi.org/10.1016/j.earlhumdev.2014.06.009

**Liu P,** Huang H, Rollins N, Chalak LF, Jeon T, Halovanic C, Lu H (2014b) Quantitative assessment of global cerebral metabolic rate of oxygen (CMRO2) in neonates using MRI. *NMR Biomed* **27**:332-340 https://doi.org/10.1002/nbm.3067

**Mallard C,** Vexler Z (2015) Modeling ischemia in the immature brain: how translational are animal models?. *Stroke* **46**:3006-3011 https://doi.org/10.1161/STROKEAHA.115.007776

**Murphy MP** (2009) How mitochondria produce reactive oxygen species. *Biochem J* **417**:1-13 https://doi.org/10.1042/BJ20081386

**Niatsetskaya ZV,** Sosunov SA, Matsiukevich D, Utkina-Sosunova IV, Ratner VI, Starkov AA, Ten VS (2012) The oxygen free radicals originating from mitochondrial complex I contribute to oxidative brain injury following hypoxia-ischemia in neonatal mice. *J Neurosci* **32**:3235-3244 https://doi.org/10.1523/JNEUROSCI.6303-11.2012

**Paradies G,** Paradies V, Ruggiero FM, Petrosillo G (2018) Mitochondrial bioenergetics and cardiolipin alterations in myocardial ischemia-reperfusion injury: implications for pharmacological cardioprotection. *Am J Physiol Heart Circ Physiol* **315**:H1341-H1352 https://doi.org/10.1152/ajpheart.00028.2018

**Paulson OB,** Hasselbalch SG, Rostrup E, Knudsen GM, Pelligrino D (2010) Cerebral blood flow response to functional activation. *J Cereb Blood Flow Metab* **30**:2-14 https://doi.org/10.1038/jcbfm.2009.188

**Piilgaard H,** Lauritzen M (2009) Persistent increase in oxygen consumption and impaired neurovascular coupling after spreading depression in rat neocortex. *J Cereb Blood Flow Metab* **29**:1517-1527 https://doi.org/10.1038/jcbfm.2009.73

**Rolfe DF,** Brown GC (1997) Cellular energy utilization and molecular origin of standard metabolic rate in mammals. *Physiological Reviews* **77**:731-758 https://doi.org/10.1152/physrev.1997.77.3.731

**Salford LG,** Siesjö BK (1974) The influence of arterial hypoxia and unilateral carotid artery occlusion upon regional blood flow and metabolism in the rat brain. *Acta Physiol Scand* **92**:130-141 https://doi.org/10.1111/j.1748-1716.1974.tb05729.x

**Sciortino VM,** Tran A, Sun N, Cao R, Sun T, Sun Y-Y, Yan P, Zhong F, Zhou Y, Kuan C-Y, *et al.* (2021) Longitudinal cortex-wide monitoring of cerebral hemodynamics and oxygen metabolism in awake mice using multi-parametric photoacoustic microscopy. *J Cereb Blood Flow Metab* **41**:3187-3199 https://doi.org/10.1177/0271678X211034096

**Sheldon RA,** Windsor C, Ferriero DM (2018) Strain-Related Differences in Mouse Neonatal Hypoxia-Ischemia. *Dev Neurosci* **40**:490-496 https://doi.org/10.1159/000495880

**Slupe AM,** Kirsch JR (2018) Effects of anesthesia on cerebral blood flow, metabolism, and neuroprotection. *J Cereb Blood Flow Metab* **38**:2192-2208 https://doi.org/10.1177/0271678X18789273

**Starkov AA,** Fiskum G (2003) Regulation of brain mitochondrial H2O2 production by membrane potential and NAD(P)H redox state. *J Neurochem* **86**:1101-1107 https://doi.org/10.1046/j.1471-4159.2003.01908.x

**Sun N,** Ning B, Bruce AC, Cao R, Seaman SA, Wang T, Fritsche Danielson R, Carlsson LG, Peirce SM, Hu S (2020) In vivo imaging of hemodynamic redistribution and arteriogenesis across microvascular network. *Microcirculation* **27**:e12598 https://doi.org/10.1111/micc.12598

**Thorngren-Jerneck K,** Ohlsson T, Sandell A, Erlandsson K, Strand SE, Ryding E, Svenningsen NW (2001) Cerebral glucose metabolism measured by positron emission tomography in term newborn infants with hypoxic ischemic encephalopathy. *Pediatr Res* **49**:495-501 https://doi.org/10.1203/00006450-200104000-00010

**Tsuji M,** Naruse H, Volpe J, Holtzman D (1995) Reduction of cytochrome aa3 measured by near-infrared spectroscopy predicts cerebral energy loss in hypoxic piglets. *Pediatr Res* **37**:253-259 https://doi.org/10.1203/00006450-199503000-00001

**Vestergaard MB,** Lindberg U, Aachmann-Andersen NJ, Lisbjerg K, Christensen SJ, Law I, Rasmussen P, Olsen NV, Larsson HBW (2016) Acute hypoxia increases the cerebral metabolic rate - a magnetic resonance imaging study. *J Cereb Blood Flow Metab* **36**:1046-1058 https://doi.org/10.1177/0271678X15606460

**Yager JY,** Brucklacher RM, Vannucci RC (1992) Cerebral energy metabolism during hypoxia-ischemia and early recovery in immature rats. *Am J Physiol* **262**:H672-677 https://doi.org/10.1152/ajpheart.1992.262.3.H672

**Yang D,** Nemkul N, Shereen A, Jone A, Dunn RS, Lawrence DA, Lindquist D, Kuan C-Y (2009) Therapeutic administration of plasminogen activator inhibitor-1 prevents hypoxic-ischemic brain injury in newborns. *J Neurosci* **29**:8669-8674 https://doi.org/10.1523/JNEUROSCI.1117-09.2009

# Peer reviews

## Reviewer #1 (Public review):

Summary:

This manuscript addresses the important problem of the uncoupling of oxidative phosphorylation due to hypoxia-ischemia injury in the neonatal brain and provides insight into the neuroprotective mechanisms of hypothermia treatment.

Strengths:

The authors used a combination of in vivo imaging of awake P10 mice and experiments on isolated mitochondria to assess various key parameters of brain metabolism during hypoxia-ischemia with and without hypothermia treatment. This unique approach resulted in a comprehensive data set that provides solid evidence to support the derived conclusions.

Weaknesses:

Several potential weaknesses were identified in the original submission, which the authors subsequently addressed in the revised manuscript. Here is the brief list of the questions:

(1) Is it possible that the observed relatively low baseline OEF and trends of increased OEF and CBF over several hours after the imaging start were partially due to slow recovery from anesthesia?

(2) What was the pain management, and is there a possibility that some of the observations were influenced by the pain-reducing drugs or their absence?

(3) Were P10 mice significantly stressed during imaging in the awake state because they didn't have head-restraint habituation training?

(4) Considering high metabolism and blood flow in the cortex, it could be potentially challenging to predict cortical temperature based on the skull temperature, particularly in the deeper part of the cortex.

(5) The map of estimated CMRO2 looks quite heterogeneous across the brain surface. Could this be partially resulting from the measurement artefact?

(6) It would be beneficial to provide more detailed justification for using P10 mice in the experiments.

https://doi.org/10.7554/eLife.100129.2.sa2

## Reviewer #3 (Public review):

Sun et al. present a comprehensive study using a novel photoacoustic microscopy setup and mitochondrial analysis to investigate the impact of hypoxia-ischemia (HI) on brain metabolism and the protective role of therapeutic hypothermia. The authors elegantly demonstrate three connected findings: (1) HI initially suppresses brain metabolism, (2) subsequently triggers a metabolic surge linked to oxidative phosphorylation uncoupling and brain damage, and (3) therapeutic hypothermia mitigates HI-induced damage by blocking this surge and reducing mitochondrial stress.

The study's design and execution are great, with a clear presentation of results and methods. Data is nicely presented, and methodological details are thorough.

However, a minor concern is the extensive use of abbreviations, which can hinder readability. As all the abbreviations are introduced in the text, their overuse may render the text hard to read to non-specialist audiences. Additionally, sharing the custom Matlab and other software scripts online, particularly those used for blood vessel segmentation, would be a valuable resource for the scientific community. In addition, while the study focuses on the short-term effects of HI, exploring the long-term consequences and definitively elucidating HI's impact on mitochondria would further strengthen the manuscript's impact.

Despite these minor points, this manuscript is very interesting.

Comments on revisions:

All addressed.

https://doi.org/10.7554/eLife.100129.2.sa1

## Author response:

The following is the authors' response to the original reviews.

> ***Reviewer #1 (Public review)***
>
> *(1) This manuscript addresses an important problem of the uncoupling of oxidative phosphorylation due to hypoxia-ischemia injury of the neonatal brain and provides insight into the neuroprotective mechanisms of hypothermia treatment.*
>
> *The authors used a combination of in vivo imaging of awake P10 mice and experiments on isolated mitochondria to assess various key parameters of the brain metabolism during hypoxia-ischemia with and without hypothermia treatment. This unique approach resulted in a comprehensive data set that provides solid evidence for the derived conclusions*

We thank the reviewer for the positive feedback.

> *(2) The experiments were performed acutely on the same day when the surgery was performed. There is a possibility that the physiology of mice at the time of imaging was still affected by the previously applied anesthesia. This is particularly of concern since the duration of anesthesia was relatively long. Is it possible that the observed relatively low baseline OEF (~20%) and trends of increased OEF and CBF over several hours after the imaging start were partially due to slow recovery from prolonged anesthesia? The potential effects of long exposure to anesthesia before imaging experiments were not discussed.*

We thank the reviewer for this important comment and for pointing out the potential influence of anesthesia on the physiological state of the animals. We apologize for any confusion. To clarify, all PAM imaging experiments were conducted in awake animals. Isoflurane anesthesia was used only during two brief surgical procedures: (1) the installation of the head-restraint plastic head plate and (2) the right common carotid artery (CCA) ligation. Each anesthesia session lasted less than 20 minutes.

We have revised the Methods section to provide additional details:

For the subsection Procedures for PAM Imaging on page 17, we clarified the sequence of procedures during the head plate installation, as well as the corresponding anesthesia duration:

"After the applied glue was solidified (~20 min), the animal was first returned to its cage for full recovery from anesthesia, and then carefully moved to the treadmill and secured to the metal arm-piece with two #4–40 screws for awake PAM imaging. The total duration of anesthesia, including preparation and glue solidification, was approximately 20 minutes."

For the subsection Neonatal Cerebral HI and Hypothermia Treatment on page 19, we also clarified the CCA ligation procedure:

"Briefly, P10 mice of both sexes anesthetized with 2% isoflurane were subjected to the right CCA-ligation. To manage pain, 0.25% Bupivacaine was administered locally prior to the surgical procedures, which took less than 10 minutes. After a recovery period for one hour, awake mice were exposed to 10% $O_2$ for 40 minutes in a hypoxic chamber at 37 °C."

Regarding the reviewer's concern about the observed trends in OEF and CBF, we agree that residual effects of anesthesia could, in principle, influence physiological parameters. However, we believe this is unlikely in this study for the following reasons. First, all imaging was conducted in awake animals after a clearly defined recovery period. Second, the trend of increasing OEF and CBF over time was consistent across animals and aligned with expected physiological responses following hypoxic-ischemic injury. In particular, the relatively low baseline OEF (0.21 at 37°C) is consistent with our previous study (0.25; (Cao et al., 2018)). The gradual increase in CBF and OEF reflects metabolic compensation and reperfusion following hypoxia-ischemia, as previously described (Lin and Powers, 2018). Therefore, we believe the observed changes are of physiological origin rather than anesthesia-related artifacts.

> *(3) The Methods Section does not provide information about drugs administered to reduce the pain. If pain was not managed, mice could be experiencing significant pain during experiments in the awake state after the surgery. Since the imaging sessions were long (my impression based on information from the manuscript is that imaging sessions were ~4 hours long or even longer), the level of pain was also likely to change during the experiments. It was not discussed how significant and potentially evolving pain during imaging sessions could have affected the measurements (e.g., blood flow and $CMRO_2$). If mice received pain management during experiments, then it was not discussed if there are known effects of used drugs on CBF, $CMRO_2$, and lesion size after 24 hr.*

We thank the reviewer for this valuable comment regarding pain management. We confirm that local analgesia was administered to all animals prior to surgical procedures. Specifically, 0.25% Bupivacaine was applied locally before both the head-restraint plate installation and the CCA ligation. These details have now been clarified in the Methods section:

For the subsection Procedures for PAM Imaging on page 16, we added:

"To manage pain, 0.25% Bupivacaine was administered locally prior to the surgical procedures."

For the subsection Neonatal Cerebral HI and Hypothermia Treatment on page 18, we added:

"To manage pain, 0.25% Bupivacaine was administered locally prior to the surgical procedures, which took less than 10 minutes."

To our knowledge, Bupivacaine has minimal systemic effects at the dose used and is unlikely to significantly alter CBF, $CMRO_2$, or lesion development (Greenberg et al., 1998). No other analgesics (e.g., NSAIDs or opioids) were administered unless distress symptoms were observed—which did not occur in this study.

Additionally, although imaging sessions were extended (up to 2 hours), animals remained calm and showed no signs of pain or distress during or after the procedures. Throughout the experimental period (up to 24 hours post-surgery), animals were monitored for signs of discomfort (e.g., abnormal activity, breathing, or weight gain), but no additional analgesia was required. The neonatal HI procedures are considered minimally invasive, and based on our protocol and prior experience, local Bupivacaine provides effective analgesia during and after the brief surgeries. We have added a corresponding note in the Discussion section (newly added subsection: Limitations in this study, the last paragraph) on page 15:

"We observed no signs of distress or pain and did not use stress- or pain-reducing drugs during imaging. However, potential effects of stress or residual pain on CBF and $CMRO_2$ cannot be fully ruled out. Future studies could incorporate more detailed pain assessment and stress-mitigation strategies to further enhance physiological reliability."

> *(4) Animals were imaged in the awake state, but they were not previously trained for the imaging procedure with head restraint. Did animals receive any drugs to reduce stress? Our experience with well-trained young-adult as well as old mice is that they can typically endure 2 and sometimes up to 3 hours of head-restrained awake imaging with intermittent breaks for receiving the rewards before showing signs of anxiety. We do not have experience with imaging P10 mice in the awake state. Is it possible that P10 mice were significantly stressed during imaging and that their stress level changed during the imaging session? This concern about the potential effects of stress on the various measured parameters was not discussed.*

We thank the reviewer for this important comment regarding the potential effects of stress during awake imaging. The neonatal mice used in our study were P10, a stage at which animals are still physiologically immature and relatively inactive. Due to their small size and limited mobility, these animals did not struggle or show signs of distress during the imaging sessions. All animals remained calm and stable throughout the procedure, and no stress-reducing drugs were administered.

We agree that, unlike older animals, P10 mice are not amenable to prior behavioral training. However, their underdeveloped motor activity and natural docility at this stage allowed for stable head-restrained imaging without inducing overt stress responses. Although no behavioral signs of stress were observed, we acknowledge that subtle physiological effects cannot be entirely excluded. We have added a brief discussion in the Discussion section (newly added subsection: Limitations in this study, the last paragraph) on page 15:

“Lastly, for awake imaging, the small size of neonatal mice at P10 aids stability during awake PAM imaging, though it limits the feasibility of prior training, which is typically possible in older animals.”

> *(5) The temperature of the skull was measured during the hypothermia experiment by lowering the water temperature in the water bath above the animal's head. Considering high metabolism and blood flow in the cortex, it could be challenging to predict cortical temperature based on the skull temperature, particularly in the deeper part of the cortex.*

We thank the reviewer for this helpful comment and for highlighting an important technical consideration. We acknowledge that we did not directly measure intracortical tissue temperature during the hypothermia experiments. While we recognize that relying on skull temperature may have limitations—particularly in reflecting temperature changes in deeper cortical regions—this approach is consistent with clinical practice, where intracortical temperature is typically not measured. Moreover, prior studies have shown that skull or brain surface temperature generally reflects cortical thermal dynamics to a reasonable extent under controlled conditions (Kiyatkin, 2007). We have added the following note in the Discussion section (newly added subsection: Limitations in this study, the 2$^{nd}$ paragraph) on page 14:

“A technical limitation is the absence of direct intracortical temperature measurements during hypothermia; we relied on skull temperature, which may not fully capture temperature dynamics in deeper cortical layers. However, this approach aligns with clinical practice, where intracortical temperature is not typically measured. Future studies could benefit from more precise intracortical assessments.”

> *(6) The map of estimated $CMRO_2$ (Fig. 4B) looks very heterogeneous across the brain surface. Is it a coincidence that the highest $CMRO_2$ is observed within the central part of the field of view? Is there previous evidence that $CMRO_2$ in these parts of the mouse cortex could vary a few folds over a 1-2 mm distance?*

We appreciate the reviewer's insightful observation regarding the spatial heterogeneity observed in the estimated $CMRO_2$ map (Fig. 4B). This heterogeneity is not a result of scanning bias, as uniform contour scanning was performed across the entire field of view. The higher $CMRO_2$ values observed in the central region are unlikely to be artifacts and more likely reflect underlying physiological variability.

Our $CMRO_2$ estimation is based on an algorithm we previously developed and validated in other tissues. Specifically, we have successfully applied this algorithm to assess oxygen metabolism in the mouse kidney (Sun et al., 2021) and to monitor vascular adaptation and tissue oxygen metabolism during cutaneous wound healing (Sun et al., 2022). These studies demonstrated the algorithm's capability to capture spatial variations in oxygen metabolism. Although the current application to the brain is novel, the algorithm has been validated in controlled experimental settings and shown to produce consistent results. We acknowledge that the observed range of $CMRO_2$ appears relatively broad across a 1–2 mm distance; however, such heterogeneity may arise from local differences in vascular density, metabolic demand, or tissue oxygenation — all of which can vary across cortical regions, even within small spatial scales. We have added a brief note in the Discussion (Subsection: Optical $CMRO_2$ detection in neonatal care) on page 13 to acknowledge this point:

"Additionally, the spatial heterogeneity in estimated $CMRO_2$ observed in our data may reflect underlying physiological variability, including differences in vascular structure or metabolic demand across cortical regions. Future studies will aim to further validate and interpret these spatial patterns."

> *(7) The justification for using P10 mice in the experiments has not been well presented in the manuscript.*

We thank the reviewer for pointing out the need to clarify our choice of developmental stage. We chose P10 mice for our hypoxia-ischemia injury model because this stage is widely recognized as developmentally comparable to human term infants in terms of brain maturation. This approach has been validated by several previous studies (Clancy et al., 2007; Mallard and Vexler, 2015; Sheldon et al., 2018). We have added the following clarification to the Methods section (Subsection: Neonatal Cerebral HI and Hypothermia Treatment) on page 18:

"P10 mice were chosen for our experiments as they are widely used to model near-term infants in humans. At this developmental stage, the brain maturation in mice closely parallels that of near-term infants, making them an appropriate model for studying neonatal brain injury and therapeutic interventions (Clancy et al., 2007; Mallard and Vexler, 2015; Sheldon et al., 2018)."

> *(8) It was not discussed how the observations made in this manuscript could be affected by the potential discrepancy between the developmental stages of P10 mice and human babies regarding cellular metabolism and neurovascular coupling.*

We thank the reviewer for raising this important point regarding developmental differences between P10 mice and human infants. We have discussed this issue by adding the following statement to the Discussion section (newly added subsection: Limitations in this study, the 1$^{st}$ paragraph) on page 15, where we summarize the overall study design and model selection:

"While P10 mice are widely used to model near-term human infants, developmental differences in cellular metabolism and neurovascular coupling may affect the observed outcomes and limit direct clinical translation (Clancy et al., 2007; Mallard and Vexler, 2015; Sheldon et al., 2018). Nevertheless, the P10 model remains a valuable and widely accepted tool for studying neonatal hypoxia-ischemia mechanisms and evaluating therapeutic interventions."

> *(9) Regarding the brain temperature measurements, the authors should use a new cohort of mice, implant the miniature thermocouples 1 mm, 0.5 mm, and immediately below the skull in different mice, and verify the temperature in the brain cortex under conditions applied in the experiments. The same approach could be applied to a few mice undergoing 4-hr-long hypothermia treatment in a chamber, which will provide information about the brain temperature that resulted in observed protection from the injury.*

We thank the reviewer for this helpful recommendation. We fully agree that direct intracortical temperature measurement would provide more accurate insight into thermal dynamics during hypothermia treatment. However, the primary aim of this study was not to characterize the precise intracortical temperature response under hypothermic conditions, but rather to examine the effects of hypothermia on $CMRO_2$ and mitochondrial function. Due to the substantial time and resources required to perform direct intracortical temperature monitoring—and considering the technical focus of the current work—we respectfully suggest reserving such investigations for a future study specifically focused on thermal dynamics in hypoxia-ischemia models.

We have acknowledged this limitation in the subsection Limitations in this study of the Discussion on page 15, noting that skull temperature was used as an approximation of brain temperature and that this approach is consistent with clinical practice, where intracortical temperature is typically not measured. We also note that future studies may benefit from more precise assessments using intracortical probes.

> *(10) The mean values presented in Fig. 4G are much lower than the peak values in the 2D panels and potentially were calculated as the average values over the entire field of view. Please provide more details on how $CMRO_2$ was estimated and if the validity of the measurements is expected across the entire field of view. If there are parts of the field of view where the estimation of $CMRO_2$ is more reliable for technical reasons, maybe one way to compute the mean values is to restrict the usable data to the more centralized part of the field of view.*

We thank the reviewer for this thoughtful comment. We confirm that $CMRO_2$ values shown in Figure 4G were calculated as spatial averages over the entire field of view (FOV; ~5 × 3 $mm^2$) encompassing both hemicortices, as shown in Figure 1C. Regarding the observed $CMRO_2$ values, The apparent difference likely reflects a comparison between two different post-HI time points. Specifically, the ~0.5 value shown for the 37°C ipsilateral group in Figure 4G reflects the average $CMRO_2$ measured 24 hours after HI, while the ~1.5 value in Figure 2D (red line) corresponds to $CMRO_2$ during the early 0–2 hour post-HI period. The temporal difference accounts for the apparent discrepancy in magnitude. We understand the importance of consistency across the field of view and have clarified this point in the subsection Procedures for PAM Imaging in the Methods on page 17 “For the imaging field covering both hemicortices between the Bregma and Lambda of the neonatal mouse (5 × 3 $mm^2$ as shown in Figure 1C, with each hemicortex measuring 2.5 × 3 $mm^2$)”, as well as in the Figure 4 legend on page 34 “Correlation of $CMRO_2$ and post-HI brain infarction in mouse neonates at 24 hours”.

In our model and setup, $CMRO_2$ estimation is spatially robust across the FOV under standard imaging conditions. We recognize, however, that certain peripheral regions may be more prone to signal attenuation. Future refinement of region selection could further improve spatial averaging strategies. For the current study, full-FOV averaging was used consistently across all groups to maintain comparability.

> *(11) Minor: Results presented in Supplementary Tables have too many significant digits.*

Thank you for the helpful suggestion. We have revised Supplementary Tables S1 and S2 to reduce the number of significant digits and improve clarity.

> ***Reviewer #2 (Public review)***
>
> *(1) In this study, authors have hypothesized that mitochondrial injury in HIE is caused by OXPHOS-uncoupling, which is the cause of secondary energy failure in HI. In addition, therapeutic hypothermia rescues secondary energy failure. The methodologies used are state-of-the art and include PAM technique in live animal, bioenergetic studies in the isolated mitochondria, and others.*
>
> *The study is comprehensive and impressive. The article is well written and statistical analyses are appropriate.*

We thank the reviewer for the positive feedback.

> *(2) The manuscript does not discuss the limitation of this animal model study in view of the clinical scenario of neonatal hypoxia-ischemia.*

We thank the reviewer for this valuable feedback. In response, we have added a dedicated "Limitations in this study" subsection in the Discussion, where we address the potential limitations of this animal model in the context of the clinical scenario of neonatal hypoxia-ischemia in the first paragraph on page 14, including the developmental differences between P10 mice and human infants.

> *(3) I see many studies on Pubmed on bioenergetics and HI. Hence, it is unclear what is novel and what is known.*

We thank the reviewer for this important comment regarding the novelty of our study in the context of existing research on bioenergetics and hypoxia-ischemia (HI). To better clarify the novel aspects of our work, we have highlighted the relevant content in the Abstract (page 4) and Introduction (page 5). Specifically, while many studies have explored HI-related bioenergetic dysfunction, the mechanisms by which therapeutic hypothermia modulates $CMRO_2$ and mitochondrial function post-HI remain poorly understood.

Abstract on page 4: "However, it is unclear how post-HI hypothermia helps to restore the balance, as cooling reduces $CMRO_2$. Also, how transient HI leads to secondary energy failure (SEF) in neonatal brains remains elusive. Using photoacoustic microscopy, we examined the effects of HI on $CMRO_2$ in awake 10-day-old mice, supplemented by bioenergetic analysis of purified cortical mitochondria."

Introduction on page 5: "The use of awake mouse neonates avoided the confounding effects of anesthesia on CBF and $CMRO_2$ (Cao et al., 2017; Gao et al., 2017; Sciortino et al., 2021; Slupe and Kirsch, 2018). In addition, we measured the oxygen consumption rate (OCR), reactive oxygen species (ROS), and the membrane potential of mitochondria that were immediately purified from the same cortical area imaged by PAM. This dual-modal analysis enabled a direct comparison of cerebral oxygen metabolism and cortical mitochondrial respiration in the same animal. Moreover, we compared the effects of therapeutic hypothermia on oxygen metabolism and mitochondrial respiration, and correlated the extent of $CMRO_2$-reduction with the severity of infarction at 24 hours after HI. Our results suggest that blocking HI-induced OXPHOS-uncoupling is an acute effect of hypothermia and that optical detection of $CMRO_2$ may have clinical applications in HIE."

In this study, we propose that uncoupled oxidative phosphorylation (OXPHOS) underlies the secondary energy failure observed after HI, and we demonstrate that hypothermia suppresses this pathological $CMRO_2$ surge, thereby protecting mitochondrial integrity and preventing injury. Additionally, our use of photoacoustic microscopy (PAM) in awake

neonatal mice represents a novel, non-invasive approach to track cerebral oxygen metabolism, with potential clinical relevance for guiding hypothermia therapy.

> *(4) What are the limitations of ex-vivo mitochondrial studies?*

We thank the reviewer for this insightful comment. We acknowledge that ex-vivo mitochondrial assays do not fully replicate in vivo physiological conditions, as they lack systemic factors such as blood flow, cellular interactions, and intact tissue architecture. However, these assays are well-established and widely accepted in the field for evaluating mitochondrial function under controlled conditions (Caspersen et al., 2008; Niatsetskaya et al., 2012). Despite their limitations, they enable direct comparisons of mitochondrial activity across experimental groups and provide valuable mechanistic insights that complement in vivo observations.

> *(5) PAM technique limits the resolution of the image beyond 500-750 micron depth. Assessing basal ganglia may not be possible with this approach?*

We thank the reviewer for this important comment. We agree that the imaging depth of PAM is limited and may not allow assessment of deeper brain structures such as the basal ganglia. However, in our neonatal HI model—as in many clinical cases of HIE—cortical injury is typically more severe and represents a major focus for mechanistic and therapeutic investigations. The cortical regions assessed with PAM are thus highly relevant to the pathophysiology of neonatal HI. We have now acknowledged this depth limitation in the third paragraph of the newly added Limitations in this study subsection of the Discussion on page 15:

"Another limitation of this study is the restricted imaging depth of the PAM technique, which is typically less than 1 mm and therefore does not allow assessment of deeper brain structures such as the basal ganglia. However, in both our neonatal HI model and most clinical cases of neonatal hypoxia-ischemia, cortical injury tends to be more prominent and functionally significant. As such, our cortical measurements remain highly relevant for investigating the mechanisms of injury and evaluating therapeutic interventions."

> *(6) Hypothermia in present study reduces the brain temperature from 37 to 29-32 degree centigrade. In clinical set up, head temp is reduced to 33-34.5 in neonatal hypoxia ischemia. Hence a drop in temperature to 29 degrees is much lower relative to the clinical practice. How the present study with greater drop in head temperature can be interpreted for understanding the pathophysiology of therapeutic hypothermia in neonatal HIE. Moreover, in HIE model using higher temperature of 37 and dropping to 29 seems to be much different than the clinical scenario. Please discuss.*

We thank the reviewer for raising this important point regarding temperature ranges in our study. In Figure 1, we used a broader temperature range (down to 29°C) to explore the general relationship between temperature and $CMRO_2$ in uninjured neonatal mice. This experiment was not intended to model therapeutic hypothermia directly, but rather to characterize the baseline physiological responses.

For all experiments involving hypothermia as a therapeutic intervention following HI, we consistently maintained a brain temperature of 32°C, which falls within the clinically accepted mild hypothermia range for neonatal HIE (typically 33–34.5°C). We believe this temperature closely mimics clinical practice and supports the translational relevance of our findings.

> *(7) NMR was assessed ex-vivo. How does it relate to in vivo assessment. Infants admitted in Neonatal intensive Care Unit, frequently get MRI with spectroscopy. How do the MRS findings in human newborns with HIE correlate with the ex-vivo evaluation of metabolites.*

We thank the reviewer for this insightful question. While our study assessed brain metabolites ex vivo, similar metabolic changes have been observed in vivo using proton magnetic resonance spectroscopy ($^1$H-MRS) in infants with HIE. Specifically, reductions in N-acetylaspartate (NAA) — a marker of neuronal integrity — have been reported in neonates with severe brain injury, aligning with our ex vivo findings. This correlation between in vivo and ex vivo assessments supports the translational relevance of our model for studying metabolic disruption in neonatal HIE. We have added this point to the subsection Using Optically Measured $CMRO_2$ to Detect Neonatal HI Brain Injury of the Results on page 8, along with a supporting clinical reference (Lally et al., 2019):

"In addition, in vivo proton MRS in infants with HIE has also shown a reduction in NAA, particularly in cases of severe injury (Lally et al., 2019). This reduction in NAA, observed in neonatal intensive care settings, reflects neuronal and axonal loss or dysfunction and serves as a biomarker for injury severity. The alignment between our ex vivo observations and in vivo MRS findings in clinical studies reinforces the translational relevance of our model for investigating metabolic disturbances in neonatal HIE."

> ***Reviewer #3 (Public review)***
>
> *(1) In Sun et al. present a comprehensive study using a novel photoacoustic microscopy setup and mitochondrial analysis to investigate the impact of hypoxia-ischemia (HI) on brain metabolism and the protective role of therapeutic hypothermia. The authors elegantly demonstrate three connected findings: (1) HI initially suppresses brain metabolism, (2) subsequently triggers a metabolic surge linked to oxidative phosphorylation uncoupling and brain damage, and (3) therapeutic hypothermia mitigates HI-induced damage by blocking this surge and reducing mitochondrial stress.*
>
> *The study's design and execution are great, with a clear presentation of results and methods. Data is nicely presented, and methodological details are thorough.*

We thank the reviewer for the positive feedback.

> *(2) However, a minor concern is the extensive use of abbreviations, which can hinder readability. As all the abbreviations are introduced in the text, their overuse may render the text hard to read to non-specialist audiences. Additionally, sharing the custom Matlab and other software scripts online, particularly those used for blood vessel segmentation, would be a valuable resource for the scientific community. In addition, while the study focuses on the short-term effects of HI, exploring the long-term consequences and definitively elucidating HI's impact on mitochondria would further strengthen the manuscript's impact.*

We thank the reviewer for these valuable suggestions. Please find our point-by-point responses below:

Abbreviations: To improve readability, we have added a List of Abbreviations on page 3 to help readers, especially non-specialists, navigate the terminology more easily.

MATLAB Code Availability: The methodology for blood vessel segmentation was described in detail in our previous publication (Sun et al., 2020). We have now updated the subsection Quantification of Cerebral Hemodynamics and Oxygen Metabolism by PAM of the Methods on page 18 to provide additional details and have indicated that the MATLAB scripts are available upon request.

"Briefly, this process involves generating a vascular map using signal amplitude from the Hilbert transformation, selecting a region slightly larger than the vessel of interest, and applying Otsu's thresholding method to remove background pixels. Isolated or spurious

boundary fragments are then removed to improve boundary smoothness. The customized MATLAB code used for vessel segmentation is available upon request."

Long-Term Effects of Hypothermia: We agree that exploring long-term outcomes would enhance the broader impact of this research. While our study focuses on the acute phase following HI, prior studies have shown long-term neuroprotective benefits of therapeutic hypothermia, such as enhanced white matter development (Koo et al., 2017). We have added this point to the fourth paragraph in the subsection Limitations in this study of the Discussion on page 15:

"While our study focuses on the acute effects of hypothermia, previous research has shown long-term neuroprotective benefits, including improved white matter development post-injury (Koo et al., 2017). These findings highlight hypothermia's potential for both immediate and extended recovery, warranting further study of long-term outcomes."

> *(3) Extensive use of abbreviations.*

Thank you for the helpful suggestion. To improve readability for a broader audience, we have added a List of Abbreviations on page 3 of the manuscript to assist readers in navigating terminology used throughout the text. This has been included as Response #2 to Reviewer #3.

> *(4) Share code used to conduct the study.*

Thank you for the suggestion. The methodology for vessel segmentation was previously published (Sun et al., 2020), and we have noted in the subsection Quantification of Cerebral Hemodynamics and Oxygen Metabolism by PAM of the Methods on page 18 that the MATLAB code is available upon request. This has also been included as Response #2 to Reviewer #3.

Reference:

Cao R, Li J, Kharel Y, Zhang C, Morris E, Santos WL, Lynch KR, Zuo Z, Hu S. 2018. Photoacoustic microscopy reveals the hemodynamic basis of sphingosine 1-phosphate-induced neuroprotection against ischemic stroke. Theranostics 8:6111–6120. doi:10.7150/thno.29435

Caspersen CS, Sosunov A, Utkina-Sosunova I, Ratner VI, Starkov AA, Ten VS. 2008. An Isolation Method for Assessment of Brain Mitochondria Function in Neonatal Mice with Hypoxic-Ischemic Brain Injury. Developmental Neuroscience 30:319–324. doi:10.1159/000121416

Clancy B, Kersh B, Hyde J, Darlington RB, Anand KJS, Finlay BL. 2007. Web-based method for translating neurodevelopment from laboratory species to humans. Neuroinformatics 5:79–94. doi:10.1385/ni:5:1:79

Greenberg RS, Zahurak M, Belden C, Tunkel DE. 1998. Assessment of oropharyngeal distance in children using magnetic resonance imaging. Anesth Analg 87:1048–1051. doi:10.1097/00000539-199811000-00014

Kiyatkin EA. 2007. Brain temperature fluctuations during physiological and pathological conditions. Eur J Appl Physiol 101:3–17. doi:10.1007/s00421-007-0450-7

Koo E, Sheldon RA, Lee BS, Vexler ZS, Ferriero DM. 2017. Effects of therapeutic hypothermia on white matter injury from murine neonatal hypoxia-ischemia. Pediatr Res 82:518–526. doi:10.1038/pr.2017.75

Lally PJ, Montaldo P, Oliveira V, Soe A, Swamy R, Bassett P, Mendoza J, Atreja G, Kariholu U, Pattnayak S, Sashikumar P, Harizaj H, Mitchell M, Ganesh V, Harigopal S, Dixon J, English P, Clarke P, Muthukumar P, Satodia P, Wayte S, Abernethy LJ, Yajamanyam K, Bainbridge A, Price D, Huertas A, Sharp DJ, Kalra V, Chawla S, Shankaran S, Thayyil S, MARBLE consortium.

2019. Magnetic resonance spectroscopy assessment of brain injury after moderate hypothermia in neonatal encephalopathy: a prospective multicentre cohort study. Lancet Neurol 18:35–45. doi:10.1016/S1474-4422(18)30325-9

Lin W, Powers WJ. 2018. Oxygen metabolism in acute ischemic stroke. J Cereb Blood Flow Metab 38:1481–1499. doi:10.1177/0271678X17722095

Mallard C, Vexler Z. 2015. Modeling ischemia in the immature brain: how translational are animal models? Stroke 46:3006–3011. doi:10.1161/STROKEAHA.115.007776

Niatsetskaya ZV, Sosunov SA, Matsiukevich D, Utkina-Sosunova IV, Ratner VI, Starkov AA, Ten VS. 2012. The Oxygen Free Radicals Originating from Mitochondrial Complex I Contribute to Oxidative Brain Injury Following Hypoxia–Ischemia in Neonatal Mice. J Neurosci 32:3235–3244. doi:10.1523/JNEUROSCI.6303-11.2012

Sheldon RA, Windsor C, Ferriero DM. 2018. Strain-Related Differences in Mouse Neonatal Hypoxia-Ischemia. Dev Neurosci 40:490–496. doi:10.1159/000495880

Sun N, Bruce AC, Ning B, Cao R, Wang Y, Zhong F, Peirce SM, Hu S. 2022. Photoacoustic microscopy of vascular adaptation and tissue oxygen metabolism during cutaneous wound healing. Biomed Opt Express, BOE 13:2695–2706. doi:10.1364/BOE.456198

Sun N, Ning B, Bruce AC, Cao R, Seaman SA, Wang T, Fritsche-Danielson R, Carlsson LG, Peirce SM, Hu S. 2020. In vivo imaging of hemodynamic redistribution and arteriogenesis across microvascular network. Microcirculation 27:e12598. doi:10.1111/micc.12598

Sun N, Zheng S, Rosin DL, Poudel N, Yao J, Perry HM, Cao R, Okusa MD, Hu S. 2021. Development of a photoacoustic microscopy technique to assess peritubular capillary function and oxygen metabolism in the mouse kidney. Kidney International 100:613–620. doi:10.1016/j.kint.2021.06.018

https://doi.org/10.7554/eLife.100129.2.sa0